Breast Cancers

6

C. Tabouret-Viaud, A. Baskin, A.J. Beer, M. Eiber,
C. Gerngross, and P. Loubeyre

Contents

Breast Cancers 91
Invasive Ductal Carcinoma (IDC) 92
Recurrence of Axillary Lymph Node 94
Breast Cancer with Lymph Nodes Invasion 96
Invasive Ductal Carcinoma (IDC) 98
Bone Metastases of an IDC 100
Metastatic Axillary Lymph Node 102
Breast Implants 104
Neuroendocrine Breast Tumor 106
Multifocal IDC with Lymph Node Invasion 108
Angiosarcoma of the Breast 110
Retroareolar ILC 112
Breast Cancer in Patient with Tuberculosis 114
Triple-Negative Breast Cancer 116
References 118

C. Tabouret-Viaud (✉) • A. Baskin
Department of Imaging, Division of Nuclear Medicine
and Molecular Imaging, Geneva University Hospital,
Rue Gabrielle Perret Gentil 4, 1211 Geneva 4, Switzerland
e-mail: claire.tabouretviaud@hcuge.ch

A.J. Beer • C. Gerngross
Department of Nuclear Medicine, Klinikum Rechts der Isar,
Technische Universität München, Munich, Germany

M. Eiber
Department of Radiology, Klinikum Rechts der Isar,
Technische Universität München, Munich, Germany

P. Loubeyre
Department of Imaging, Division of Radiology,
Geneva University Hospital, Rue Gabrielle Perret Gentil 4,
1211 Geneva 4, Switzerland

Breast Cancers

Breast cancer is the leading cancer and the second leading cause of mortality in women in most European countries, North America, and Australia. In Europe, 1 out of every 10–15 women will develop breast cancer in her lifetime, and the risk is even higher in the United States, where it is 1 out of every 8 women.

MRI plays an important role in the characterization of breast lesions for patients with suspected breast cancer [1, 2], and may change the surgical approach at least for young women or women with dense breast or in cases of high risk of multifocal/multicentric lesions [3]. However, MRI's positive predictive value and specificity vary over a wide range [4]. 18F-FDG whole body PET/CT on the contrary is highly specific [4], and stages not only axillary and internal mammary nodes but also the whole body for unexpected sites of disease. Its utility as a staging procedure in primary stage II and III breast cancer has now been proven [5], as well as for inflammatory breast cancers at diagnosis [6, 7]. PET/CT is also useful for detecting recurrence in breast cancer patients, for restaging [8], and for treatment response assessment [9–11]. Therefore, ^{18}F-FDG PET/CT has become more widely adopted in selected categories of patients, where PET is complementary to breast MRI resulting in both modalities to be part of patient clinical workup.

On those patients, the emergence of hybrid PET/MR scanners offers the advantage of combining both studies in a single session, reducing radiation dose of CT and allowing more accurate localization of lesion detection. Optimized whole-body PET/MR protocols, can also be acquired if necessary in addition to dedicated breast MRI using specific breast coils compatible with PET, allowing full diagnostic quality of both modalities. This could become the modality of choice in those indications, reducing the effective dose of radiation compared to PET/CT, and decreasing the total time of the examination in a single session instead of two separate exams [12].

O. Ratib et al. (eds.), *Atlas of PET/MR Imaging in Oncology*,
DOI 10.1007/978-3-642-31292-2_6, © Springer-Verlag Berlin Heidelberg 2013

Invasive Ductal Carcinoma (IDC)

Clinical History

Forty-one-year-old patient with cT2 N1a invasive ductal carcinoma, G2, of the junction of the inferior quadrants of the left breast. PET/MR was performed for staging.

Imaging Technique

Whole-body PET acquired 60 min after injection of 371 MBq of 18F-FDG, 57 kg/168 cm patient, with 3.7 mmol/L of fasting glycemia. Whole body atMR (T1 weighted), supine position.

T2 TSE axial, 3D e-thrive native, arterial and veinous post-gadolinium, and breast PET in a SENSE breast-coil, prone position.

Findings

Breast MR showed a 50 mm maximal diameter tumor of the junction of the left inferior quadrants, and a suspicious retroareolar linear enhancement. PET imaging showed a 25 mm diameter hypermetabolic suspicious area of the junction of the left inferior quadrants. No ipsilateral axillary lymph node involvement was noted. Pathological examination of left mastectomy found a 95×45×20 mm invasive ductal carcinoma of the central area of the breast. Sentinel lymph node biopsy was negative.

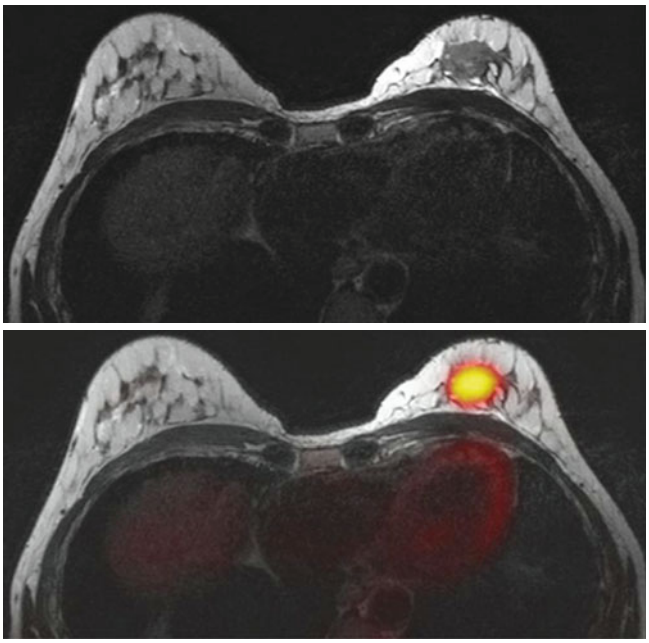

Fig. 6.1 T2 TSE axial MRI sequence acquired using dedicated breast coil (*top*), fused with PET acquired in the same PET-compatible coil (*bottom*), showing the left breast hypermetabolic lesion

Teaching Points

MRI is more effective than PET to assess tumor extent when the tumor infiltration is along the linear galactophoric channels both techniques may underestimate the tumor extension in these cases.

Fig. 6.2 Coronal MIP from whole-body PET showing cervical and supra-clavicular brown fat tracer uptake (*arrows*) for this young patient, and the breast tumor without evident distant extension

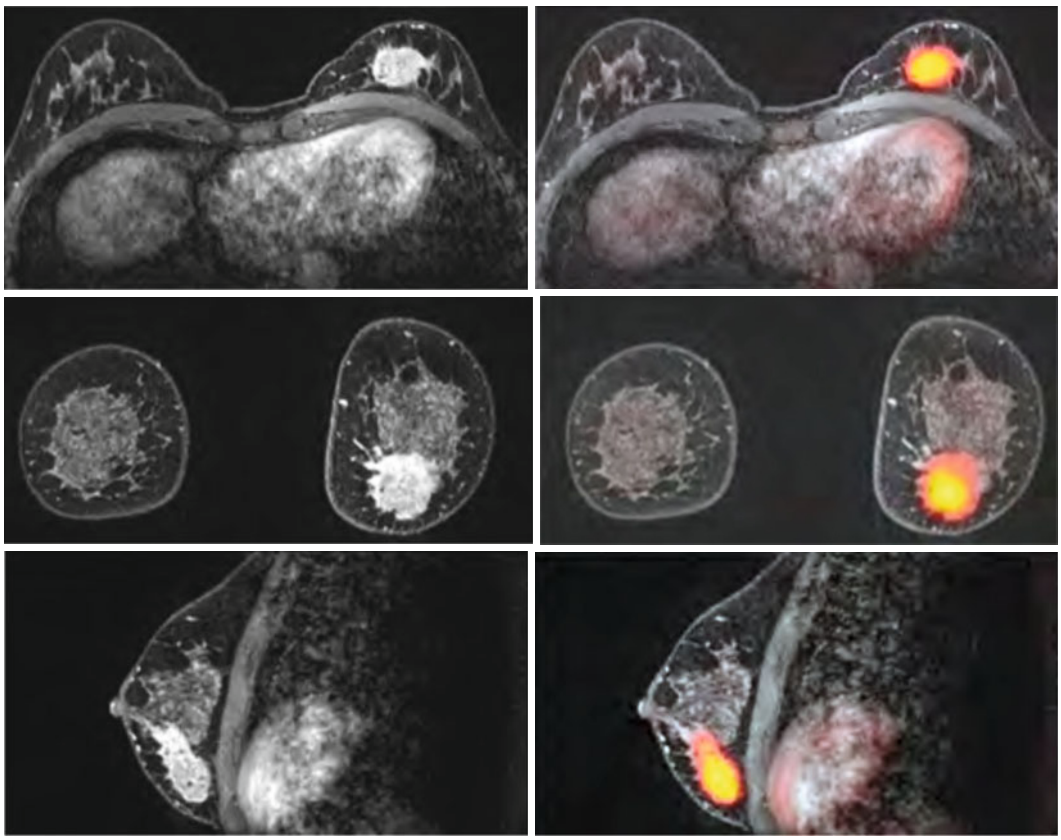

Fig. 6.3 E-thrive arterial MRI sequence in the three orthogonal planes, showing the hypermetabolism and the contrast enhancement of the single left breast lesion

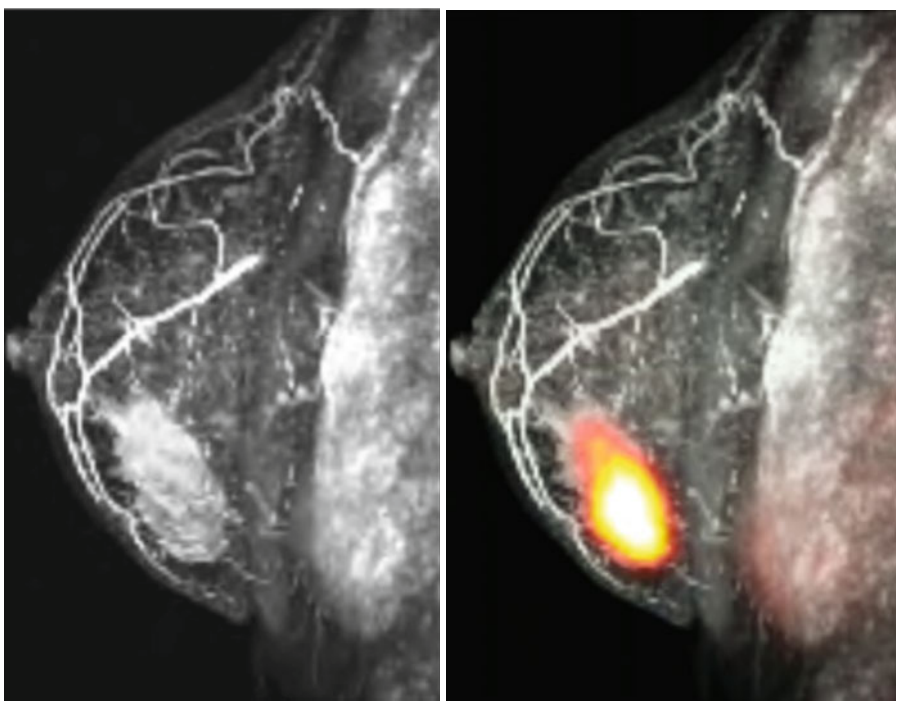

Fig. 6.4 3D volume rendering of an e-thrive arterial phase MRI sequence in a sagittal view, showing the hypermetabolism and the contrast enhancement of the single left breast lesion

Recurrence of Axillary Lymph Node

Clinical History

Sixty-four-year-old patient with history of left lumpectomy and axillary lymph node dissection 14 years ago for invasive lobular carcinoma (ILC) and tumorectomy of a right invasive ductal carcinoma with radiotherapy and chemotherapy 8 years ago. Patient presented with a clinically suspicious 2-cm single left axillary nodule.

Imaging Technique

Whole-body PET acquired 60 min after injection of 382 MBq of 18F-FDG, 70 kg patient, with 5 mmol/L of fasting glycemia. Whole body atMR (T1 weighted), supine position.

T2 TSE axial, 3D e-thrive native, arterial and venous post-gadolinium, and breast PET in a SENSE breast-coil, prone position.

Findings

PET/MR showed a 3-cm single tumoral lesion of the lower limit of the left axillary region. Subsequent pathological examination of axillary tumorectomy showed a single 28-mm G2 invasive ductal carcinoma.

Teaching Points

In this case, both MRI and PET gave the same information: they confirmed the presence of a suspicious left axillary nodule. PET provided no evidence for other metastatic lesions which is important for the surgeon. This patient already had extensive left axillary dissection and performing additional exploratory surgery can be risky and difficult. Radiotherapy of the region is indicated in the absence of axillary invasion either clinically and / or on imaging.

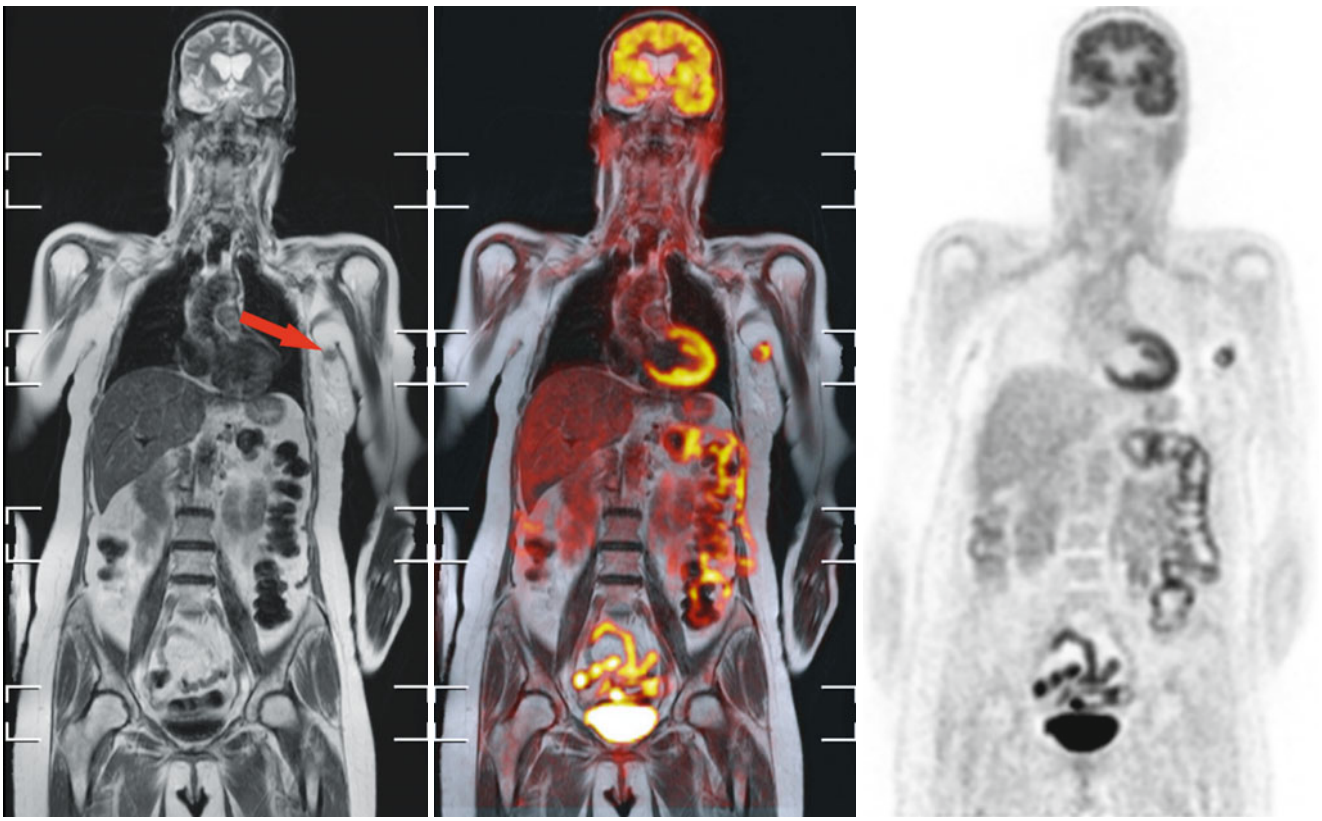

Fig. 6.5 Whole-body T2W MRI sequence fused with PET, and FDG-PET alone, *from the left to the right*, showing the main lesion in the left axillary region (*arrow*)

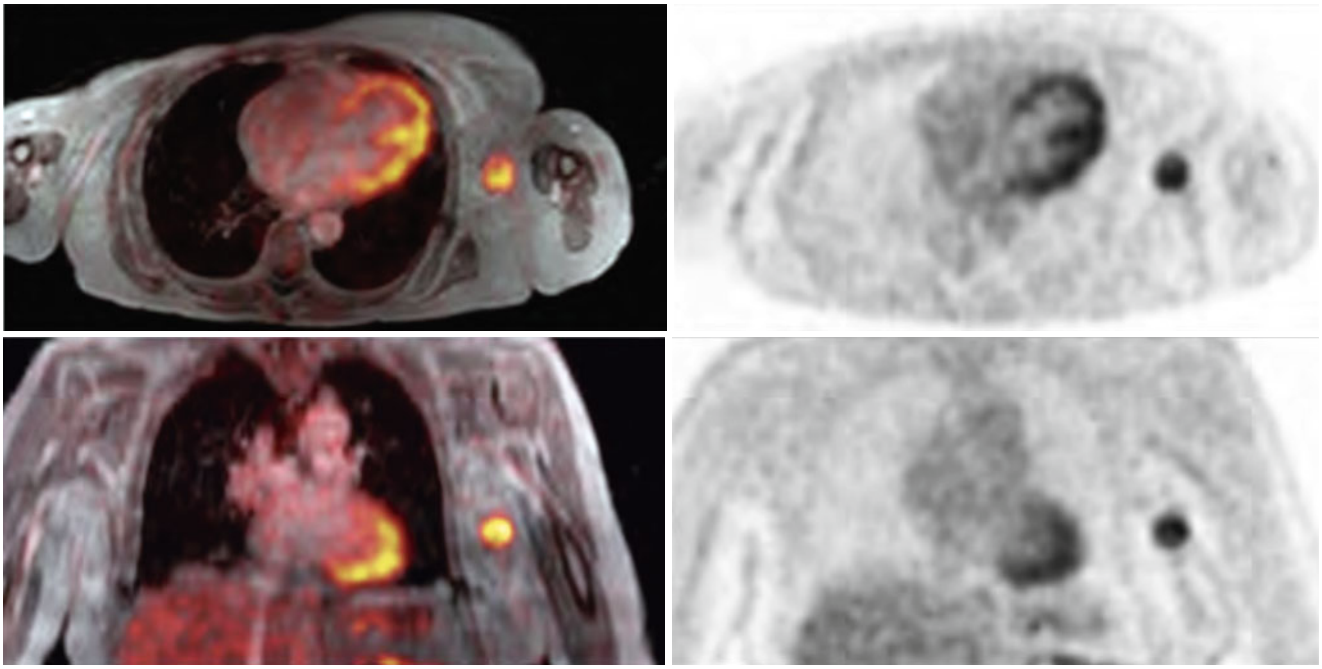

Fig. 6.6 Axial (*top*) and coronal (*bottom*) views of fused PET/MR (*left*) and PET (*right*) images centered over the left axillary region showing a single lesion with no evidence of additional axillary lymph node invasion

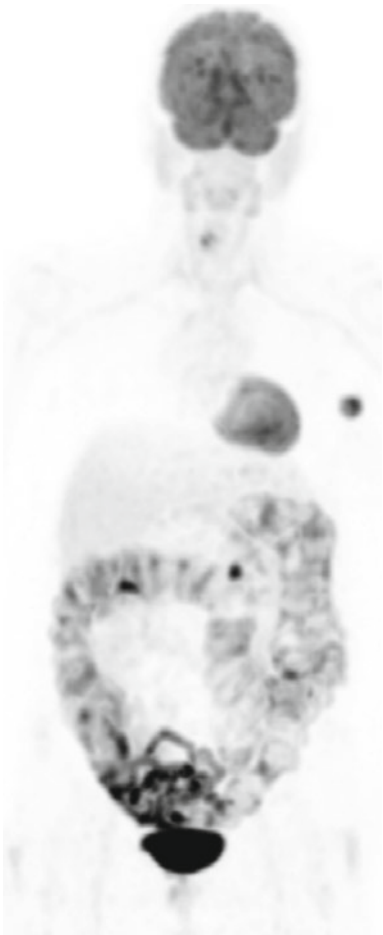

Fig. 6.7 Whole body MIP image showing the single left axillary region with no evidence of other dissemination or lymph node involvement

Breast Cancer with Lymph Nodes Invasion

Clinical History

Forty-one-year-old patient with invasive ductal carcinoma (IDC) cT4b N3b G2 of the right breast. PET/MR was performed for staging before neoadjuvant chemotherapy.

Imaging Technique

Whole-body PET acquired 60 min after injection of 375 MBq of 18F-FDG, 74 kg/177 cm patient, with 4.1 mmol/L of fasting glycemia. Whole body atMR (T1 weighted), supine position.

T2 TSE axial, T2W TSE STIR, 3D e-thrive native, arterial and venous post-gadolinium, and breast PET in a SENSE breast-coil, prone position.

Findings

PET/MR showed a right breast multifocal/multicentric carcinoma, with highly suspicious right axillary and internal mammary lymph nodes. Note a post-biopsy collection of the right inner superior quadrant. Post chemotherapy pathological examination of right mastectomy and axillary lymph node dissection showed a residual lymphangitic carcinomatosis and ductal carcinoma in-situ (DCIS) of 13-cm maximal diameter.

Teaching Points

Internal mammarian lymph node involvement is more difficult to assess on MRI compared to PET, but this information is important to adjust the radiation field of the thoracic radiotherapy after mastectomy in this case.

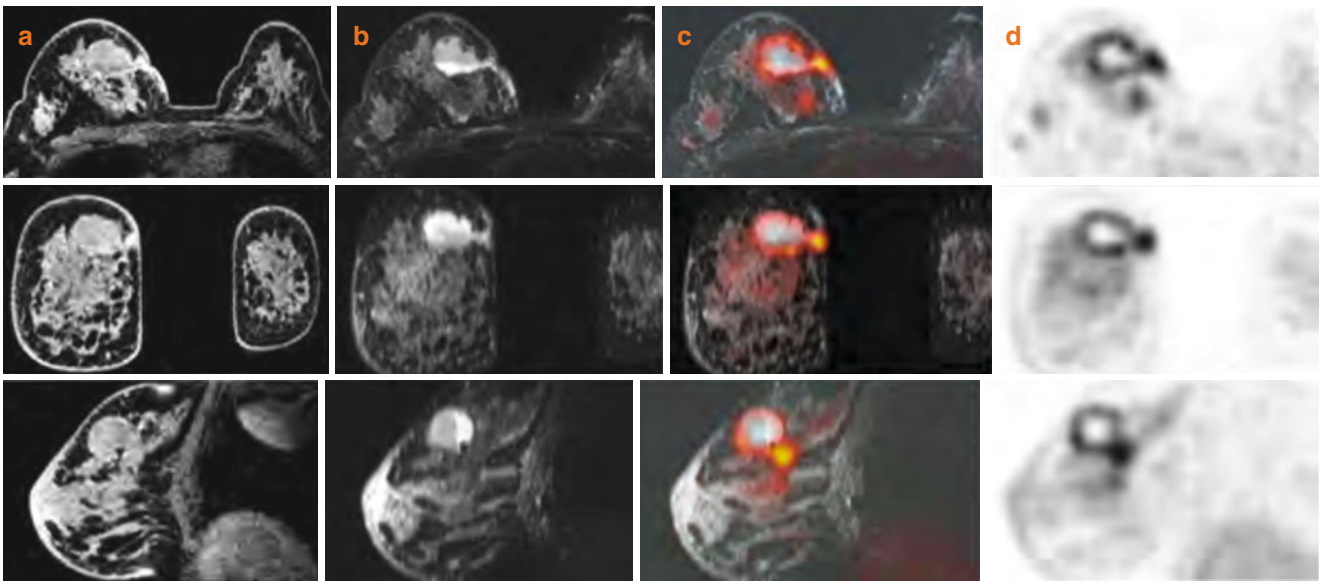

Fig. 6.8 Three orthogonal plane images showing the right breast lesion, *from left to right*: (**a**) T1 dynamic e-thrive MRI sequence; (**b**) T2 TSE STIR MRI sequence; (**c**) Fusion of PET and MRI; and (**d**) PET images

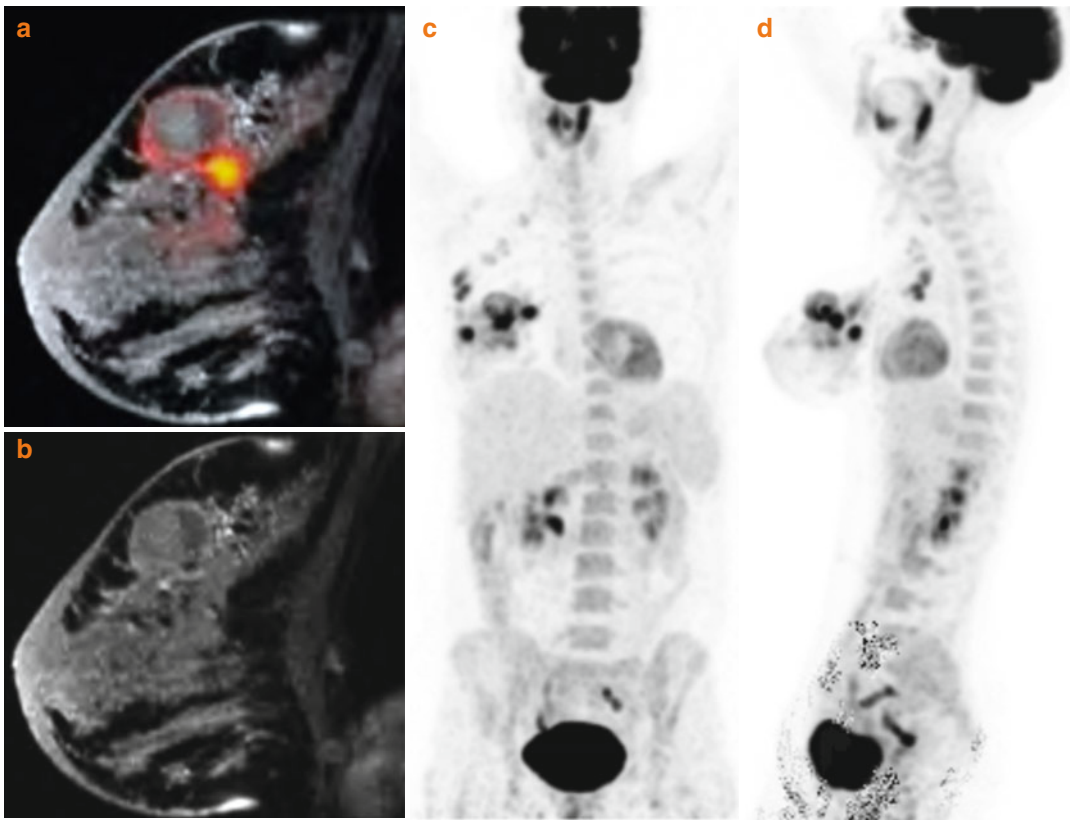

Fig. 6.9 Dynamic e-thrive MRI sequence fused with PET (**a**) and dynamic e-thrive MRI sequence alone (**b**) showing the tumor lesion and a fluid/air cavity. Coronal (**c**) and sagittal (**d**) whole body MIP images of PET showing the multifocal tumor of the left breast and the extension along the axillary and mammary lymph nodes

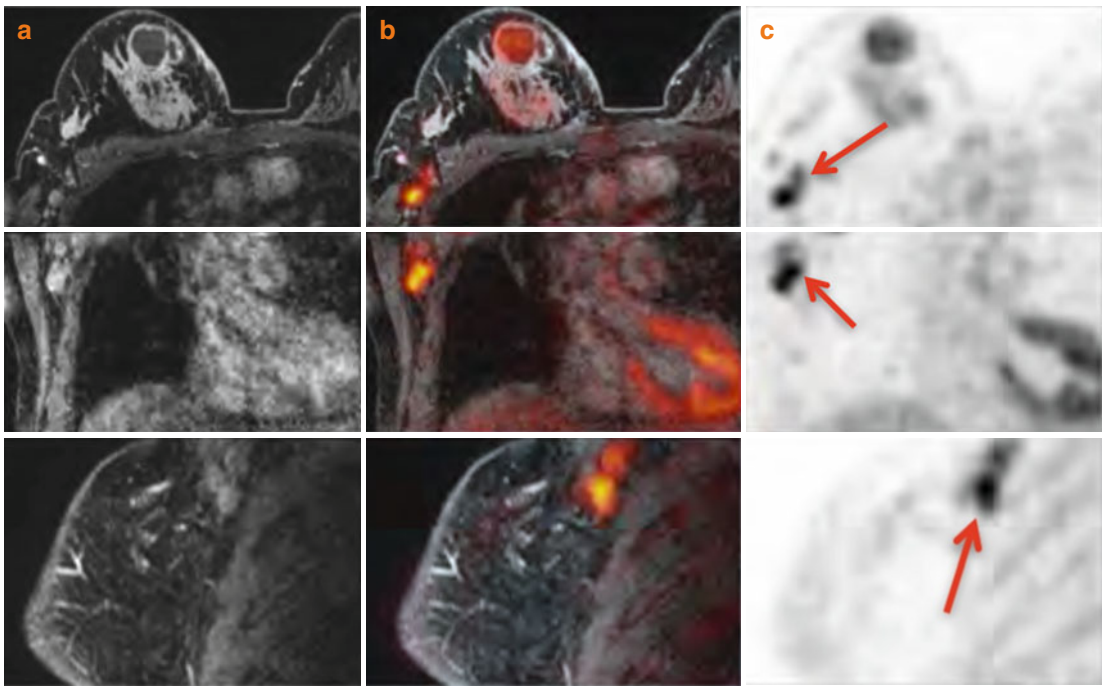

Fig. 6.10 Three orthogonal plane images showing the axillary lymph nodes with high FDG uptake (*arrows*), *from left to right*: (**a**) T1 dynamic e-thrive sense MRI sequence; (**b**) PET/MR with same MRI sequence; and (**c**) PET images

Invasive Ductal Carcinoma (IDC)

Clinical History

Forty-two-year-old patient with a G3 cT3 N1a invasive ductal carcinoma (IDC) of the junction of the superior quadrants of the left breast. PET/MR was performed for staging.

Imaging Technique

Whole-body PET acquired 60 min after injection of 380 MBq of 18F-FDG, 62 kg patient, with 5.1 mmol/L of fasting glycemia. Whole body atMR (T1 weighted), supine position.

T2 TSE axial, 3D e-thrive native, arterial and venous post-gadolinium, and breast PET in a SENSE breast-coil, prone position.

Findings

Whole body and breast PET/MR showed multifocal/bicentric tumoral involvement of the superior quadrants of the left breast with massive ipsilateral axillary lymph node invasion, without controlateral breast lesion or distant metastatic extent. Pathological examination of left mastectomy and axillary lymph node dissection showed a 40-mm (maximal diameter) invasive ductal carcinoma G3 of the left superior quadrants, with extensive peritumoral vascular invasion, retroareolar intraductal papilloma, and massive lymph node involvement (10 metastatic lymph nodes).

Teaching Points

The left axillary lymph node involvement is difficult to identify on MRI because of cardiac motion artefacts, but clearly visible on PET.

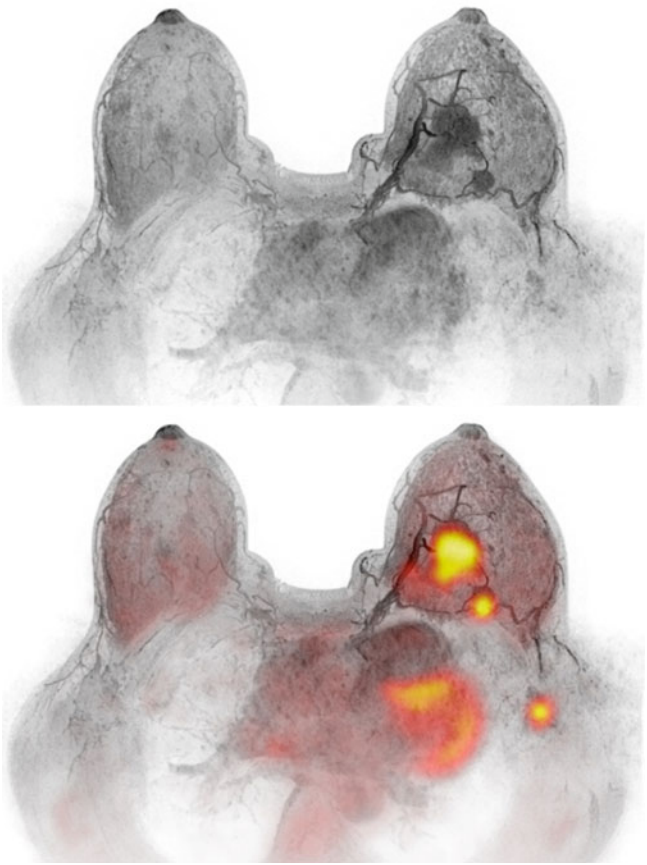

Fig. 6.11 Volume rendering of 3D arterial phase e-thrive MRI (*top*), fused with FDG-PET (*bottom*) showing multifocal tumor localization

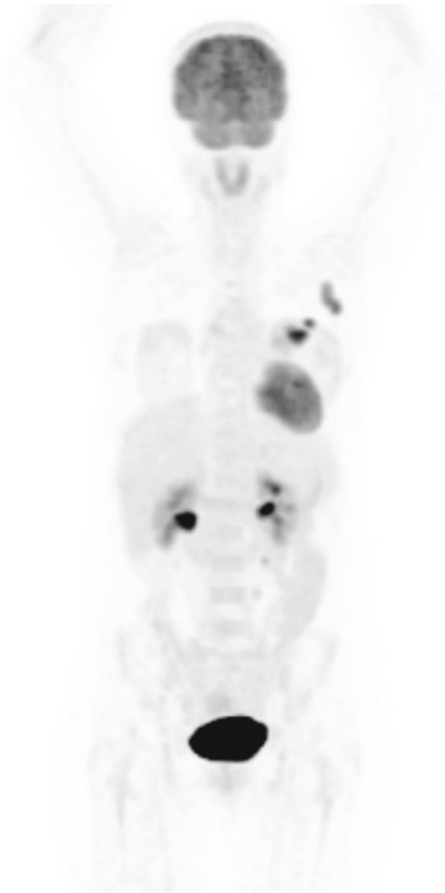

Fig. 6.12 Coronal view of the PET MIP acquired in prone position showing left breast tumor and axillary lymph node uptake of FDG

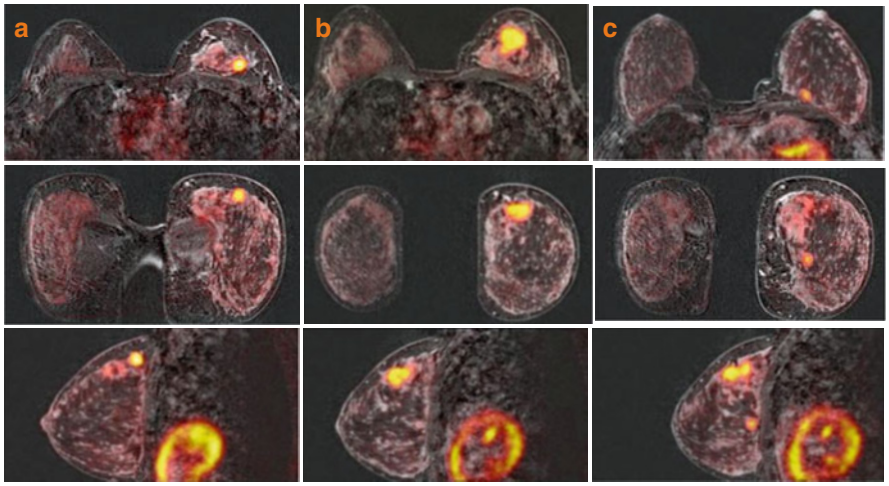

Fig. 6.13 (**a**–**c**) Three orthogonal planes of PET images fused with venous subtraction MRI sequence showing multiple primary lesions on three levels

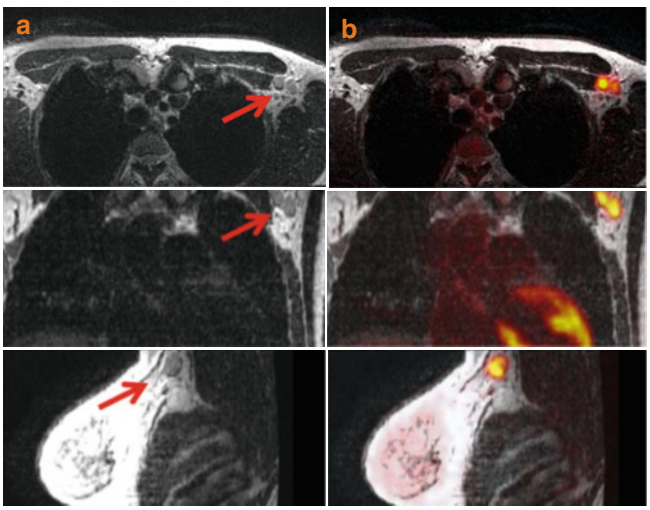

Fig. 6.14 Three orthogonal plane T2 TSE MRI sequences (**a**) and fused images with PET (**b**), showing positive axillary lymph nodes with tracer uptake (*arrow*)

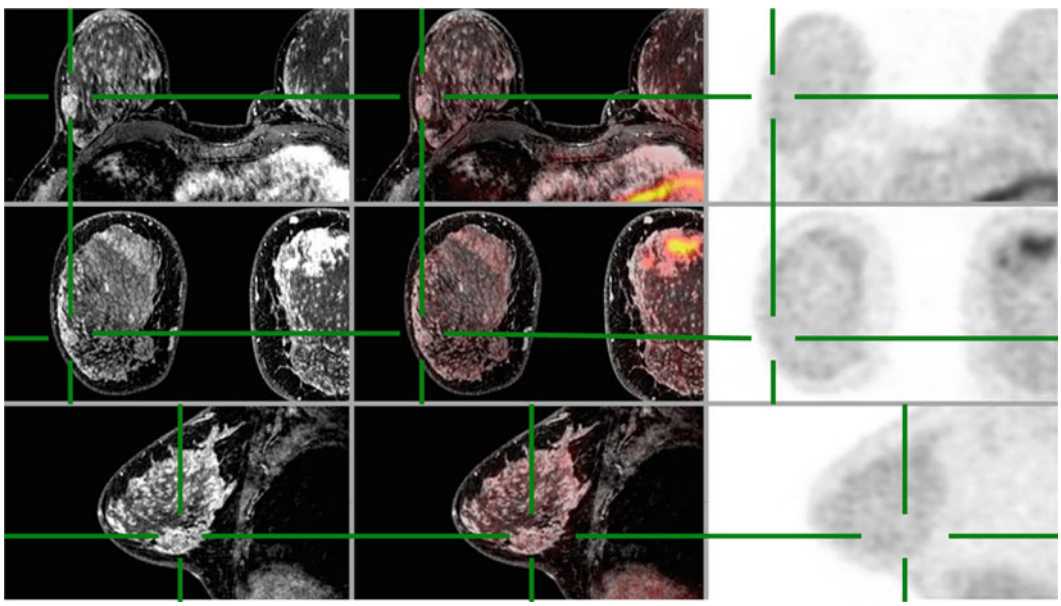

Fig. 6.15 Arterial phase of e-thrive MRI sequence showing a benign fibrocyst in the contralateral right breast with no significant FDG uptake

Bone Metastases of an IDC

Clinical History

Sixty-four-year-old patient with history of right breast invasive ductal carcinoma (IDC), diagnosed 10 years ago. Patient had bilateral mastectomy. Patient had whole body PET/MR for a suspicion of bone metastases.

Imaging Technique

Whole-body PET acquired 60 min after injection of 372 MBq of 18F-FDG, 62 kg/163 cm patient, with 4.8 mmol/L of fasting glycemia. Whole body atMR (T1 weighted), supine position.

T2 TSE axial, Total spine T1w and T2w TSE 3D e-thrive native, arterial and venous post-gadolinium, and breast PET in a SENSE breast-coil, prone position.

Findings

Whole body PET/MR showed several bone metastases including glenoid, sternum, pelvic bones and lumbar spine.

Teaching Points

Whole body PET helps confirming the presence of suspected bone metastases in different areas. Localized MRI can then be performed on suspicious areas.

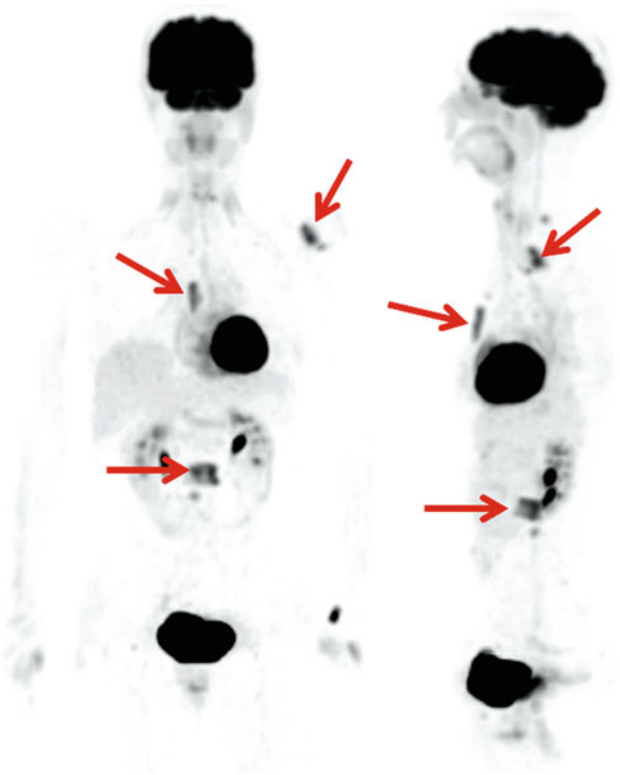

Fig. 6.16 Coronal and sagittal views of FDG-PET MIP, *arrows* showing the glenoid metastasis, sternal metastasis and lumbar vertebral metastasis

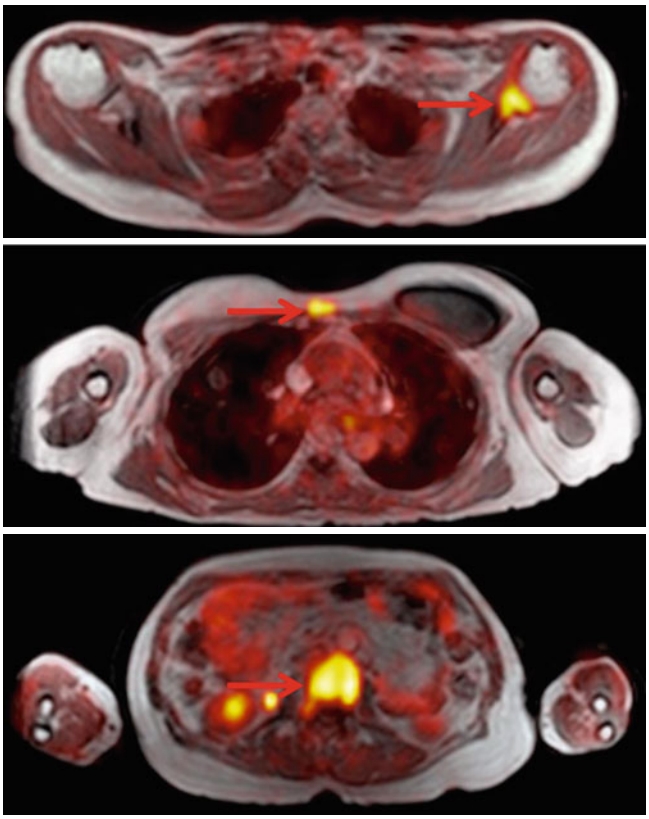

Fig. 6.17 Axial fused images of whole-body attenuation correction MRI and FDG-PET, showing the same lesions at the glenoid (*top arrow*), sternum (*middle arrow*) and L2 vertebra (*lower arrow*)

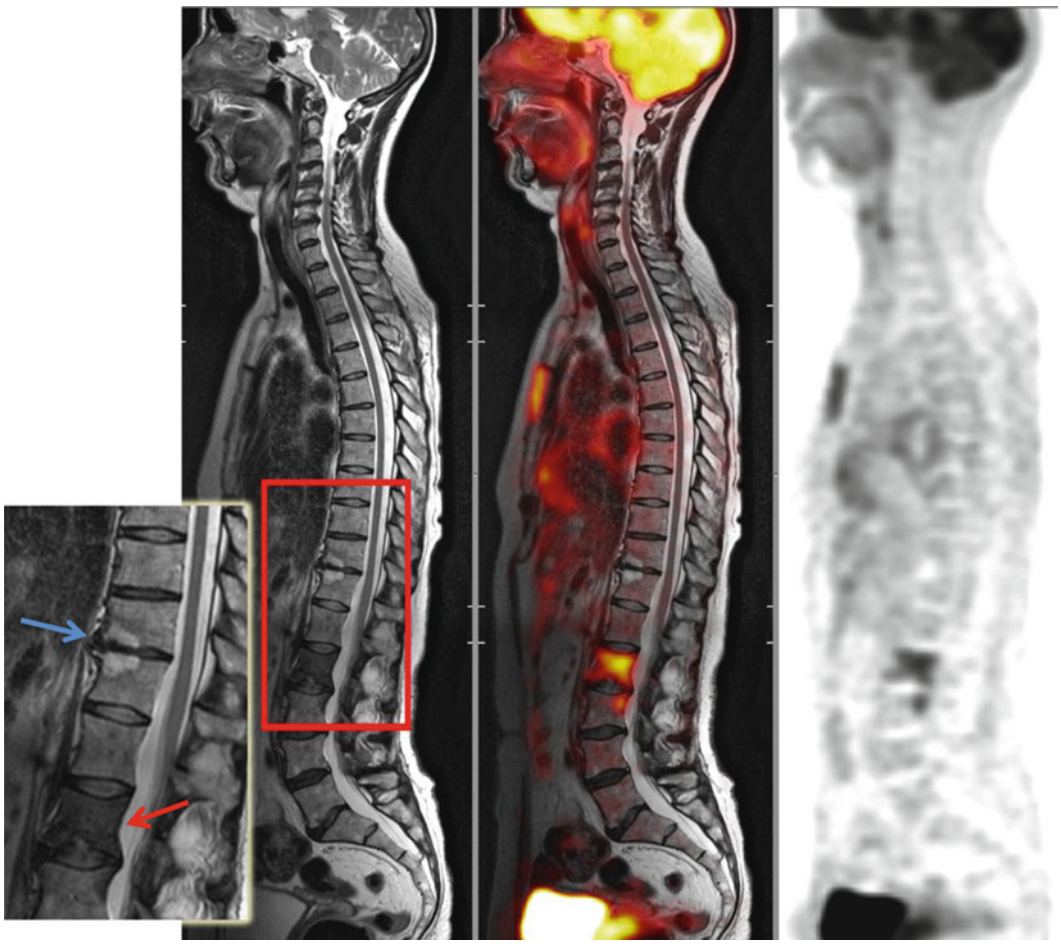

Fig. 6.18 T2W TSE MRI sequence showing vertebral metastases (*red arrow*). The *blue arrow* shows benign degenerative bone lesions with no significant FDG uptake on T11 and T12 vertebrae. The *red rectangle* shows the region that was enlarged in the inset image on the left

Fig. 6.19 T1W TSE sequence centered on the lower spine metastasis

Fig. 6.20 T2W TSE MRI sequence centered on the lower spine metastasis

Metastatic Axillary Lymph Node

Clinical History

Forty-one-year-old patient with history of right skin-sparing mastectomy with advanced breast reconstruction surgery (DIEP) 7 years ago for ductal carcinoma in situ (DCIS). Invasive ductal carcinoma was found on core-needle biopsy (CNB) of a clinically suspicious right axillary lymph node.

Imaging Technique

Whole-body PET acquired 60 min after injection of 368 MBq of 18F-FDG, 64 kg/164 cm patient, with 5.1 mmol/L of fasting glycemia. Whole-body atMR (T1 weighted), supine position.

T2 TSE axial, 3D e-thrive native, arterial and venous post-gadolinium, and breast PET in a SENSE breast-coil, prone position.

Findings

No suspicious breast lesion was found on breast PET/MR. One suspicious right axillary lymph node on MRI and three suspicious lymph nodes on PET imaging were noted. Eight nodes among 17 were metastatic on subsequent pathological examination of right axillary node dissection. Three metastatic lymph nodes presented capsular disruption.

Teaching Points

Heterogeneous contrast-enhancement of non-tumoral left breast tissue was difficult to interpret on MRI alone, but PET showed no suspicious FDG uptake in that region excluding a tumor.

Right lymph node invasion was more clearly identified on PET compared to MRI.

Fig. 6.21 Coronal whole body MIP of FDG PET study showing focal tracer uptake in the right axillary region

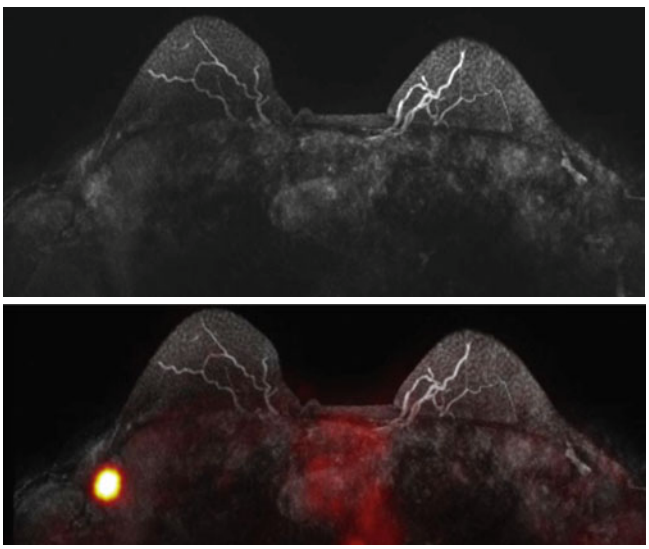

Fig. 6.22 Axial volume rendering of venous phase of MRI e-THRIVE sequence (*top*), fused with FDG-PET (*bottom*) showing absence of tracer uptake in the breast but focal uptake in the axillary region

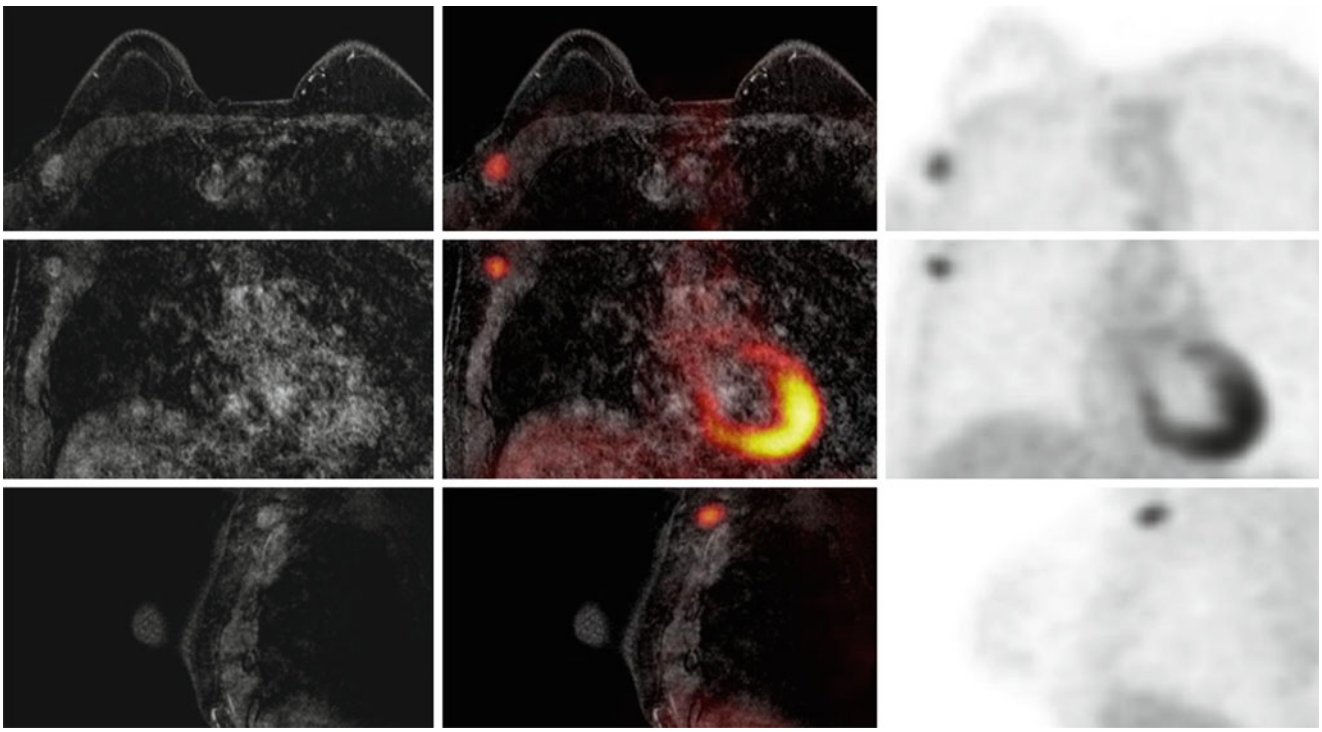

Fig. 6.23 Axial (*top*), coronal (*middle*) and sagittal (*bottom*) views of arterial phase e-THRIVE MRI sequence (*left*), fused with FDG-PET (*middle*), and FDG-PET alone (*right*), centered on the suspicious right axillary lymph node

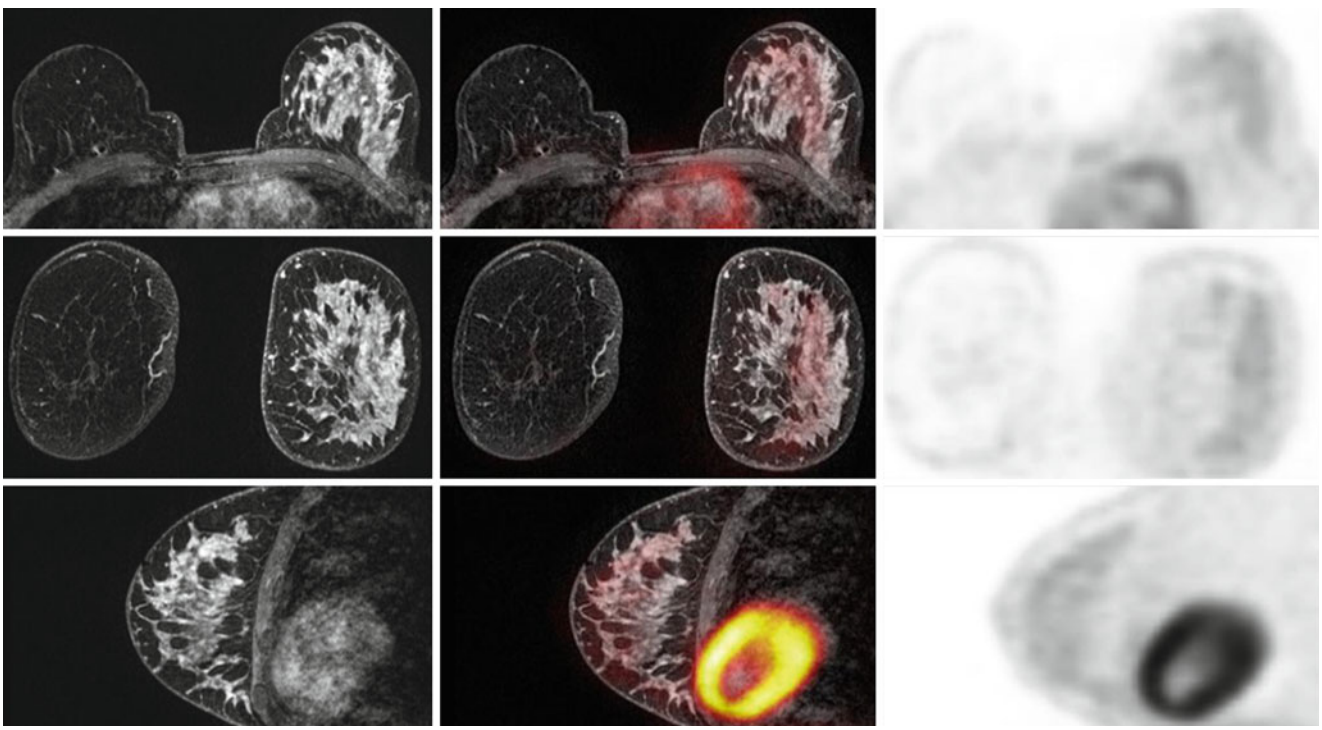

Fig. 6.24 Three orthogonal planes of T2 TSE MRI sequence (*left*) fused with FDG-PET (*middle*), and FDG-PET alone (*right*), showing no tracer uptake in the breasts, and dense left breast tissue compared to the right side, secondary to the DIEP performed 7 years earlier

Breast Implants

Clinical History

Forty-five-year-old patient with bilateral breast implants presenting with chronic inflammatory syndrome of unknown origin. Inflammatory or tumoral process was suspected.

Imaging Technique

Whole-body PET acquired 60 min after injection of 375 MBq of 18F-FDG, 58 kg/157 cm patient, with 6.5 mmol/L of fasting glycemia. Whole body atMR (T1 weighted), supine position.

T2 TSE axial, Silicone only T2w (achieved using STIR fat suppression and SPAIR water suppression) 3D e-thrive native, arterial and venous post-gadolinium, and breast PET in a SENSE breast-coil, prone position.

Findings

Breast PET/MR was interpreted as normal with no evidence of focal FDG uptake but with a small focal contrast enhancement on the right breast (see Fig. 6.27) corresponding to a benign lesion.

Teaching Points

MRI provides the high spatial and contrast resolution to assess breast implants. Small nodular contrast uptake at the retro-areolar glandular tissue is still difficult to interpret on MRI. The absence of metabolic activity in PET will help exclude the presence of a small malignant tumor.

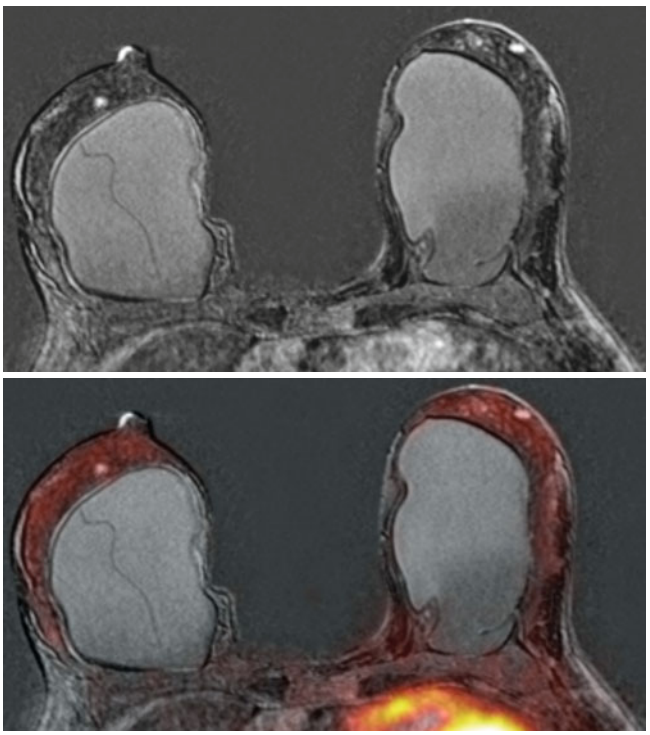

Fig. 6.25 Subtraction MRI sequence (*top*) fused with PET (*bottom*), showing neither suspicious uptake nor hypermetabolism

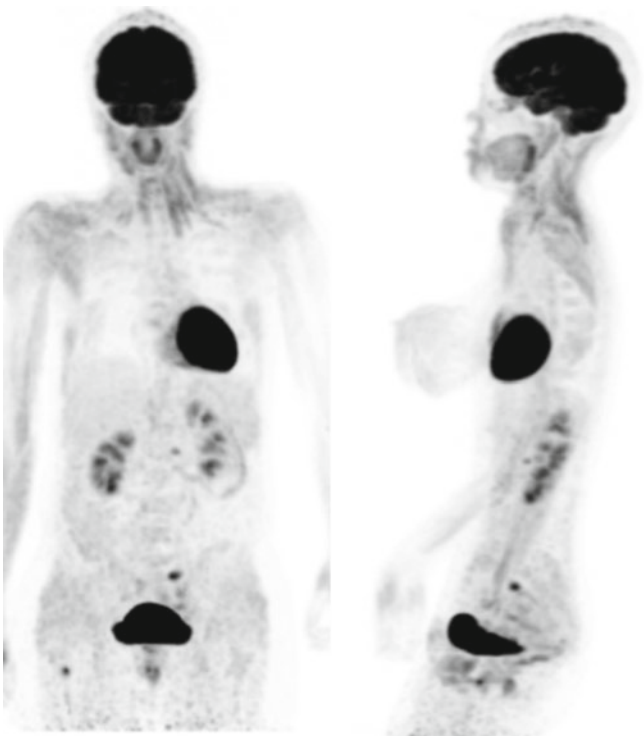

Fig. 6.26 Coronal and lateral views of the PET MIP

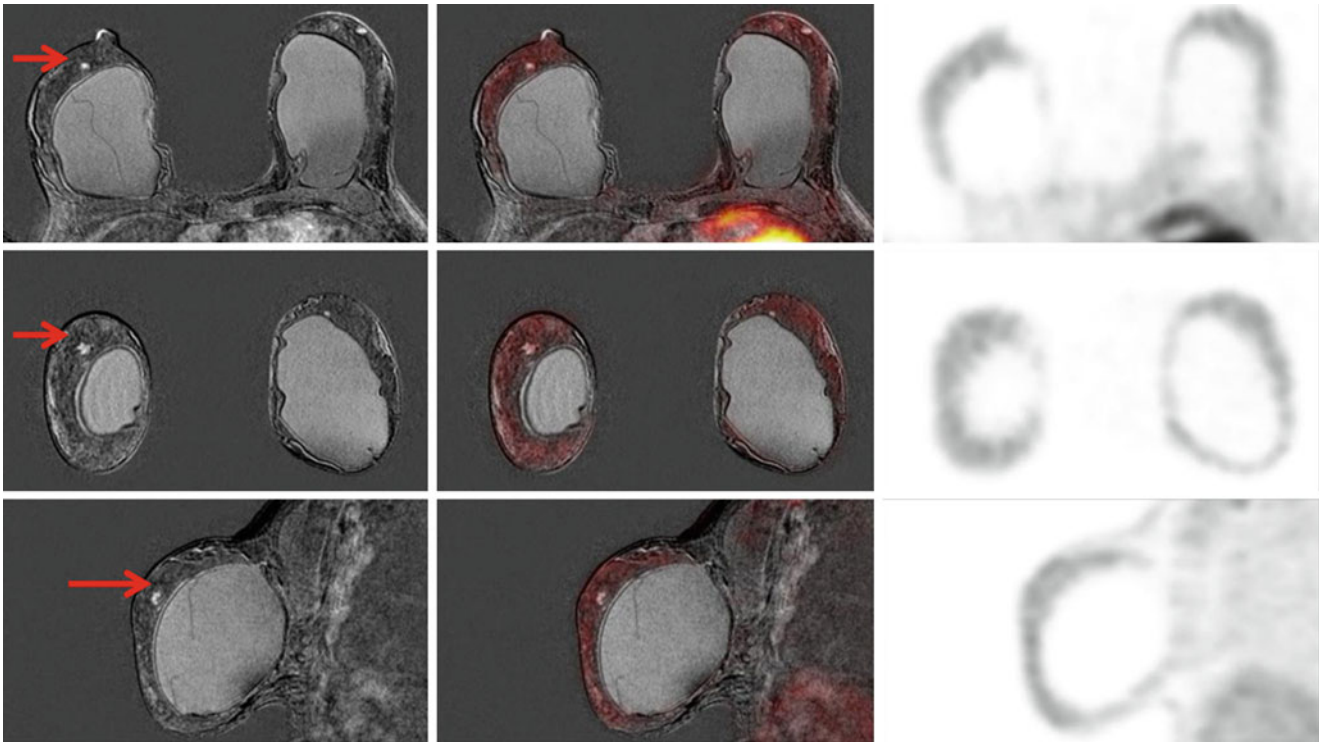

Fig. 6.27 Three orthogonal planes of subtraction e-thrive MRI sequence, fused with PET in the middle, and PET alone on the right showing small focal contrast enhancement on the right breast (*arrow*) with no significant metabolic tracer uptake

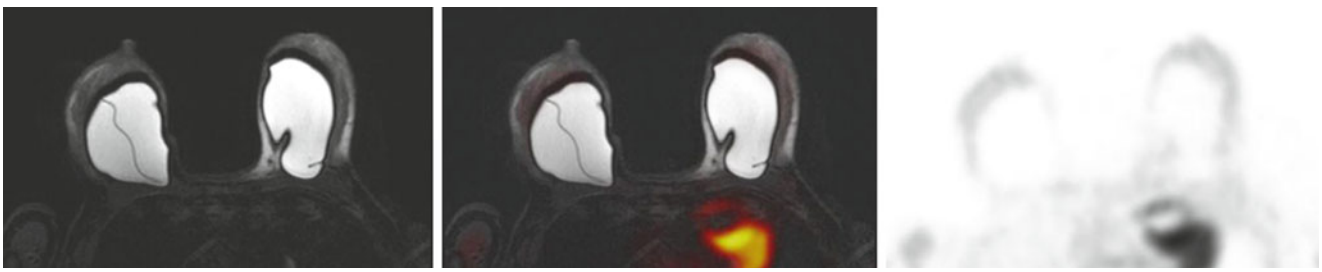

Fig. 6.28 Silicone only T2 weighted MRI sequence (*left*), fused with PET (*middle*), and PET alone (*right*)

Neuroendocrine Breast Tumor

Clinical History

18-F-DOPA PET for a 71-year-old patient with cT1 N0 neuroendocrine invasive carcinoma of the inferior outer quadrant of the left breast. Study requested for staging and evaluation of tumor extension.

Imaging Technique

Whole-body PET acquired 60 min after injection of 200 MBq of 18F-DOPA, 55 kg/158 cm patient. Whole body atMR (T1 weighted), supine position.

T2 TSE axial, 3D e-thrive native, arterial and venous post-gadolinium, and breast PET in a SENSE breast-coil, prone position.

Findings

Breast PET/MR displayed a 25-mm single tumoral lesion of the left inferior outer quadrant. Subsequent pathological examination of lumpectomy showed a 30-mm diameter tumoral lesion. No metastasis was found on PET/CT and PET/MR. Sentinel lymph node biopsy was negative.

Teaching Points

This case demonstrates the effectiveness of 18F-DOPA in characterizing a rare breast tumoral lesion, with perfect correlation of PET and MRI findings in neuroendocrine tumor.

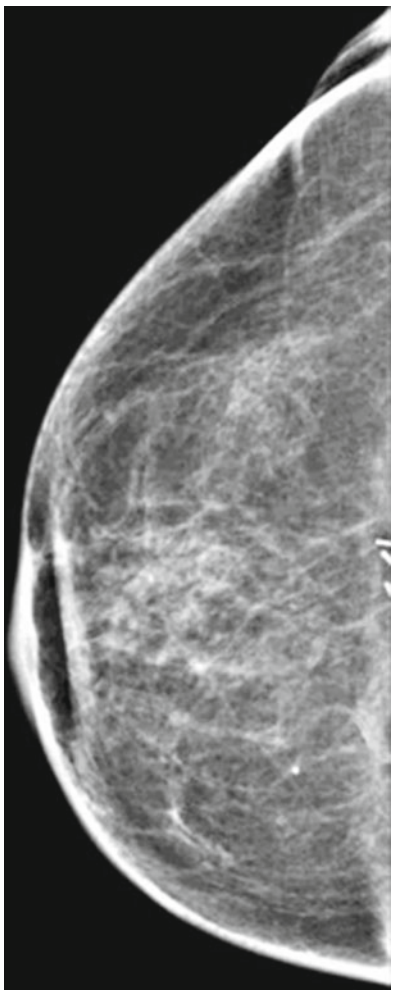

Fig. 6.29 Left mammography showing the left breast lesion

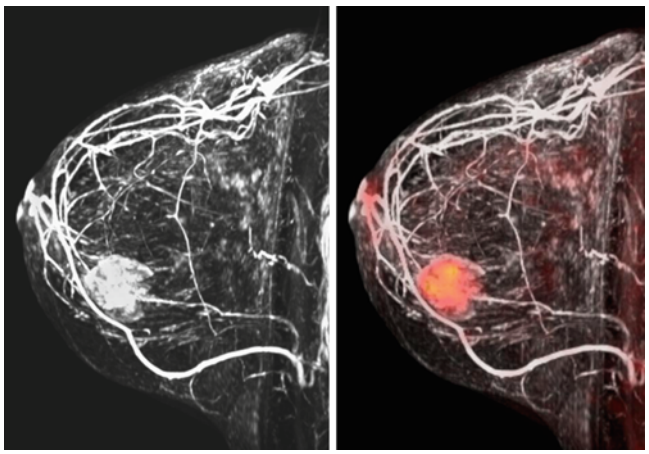

Fig. 6.30 Sagittal volume rendering of venous phase of e-thrive MRI sequence in 3D reconstruction showing the left breast lesion with 18-F DOPA uptake

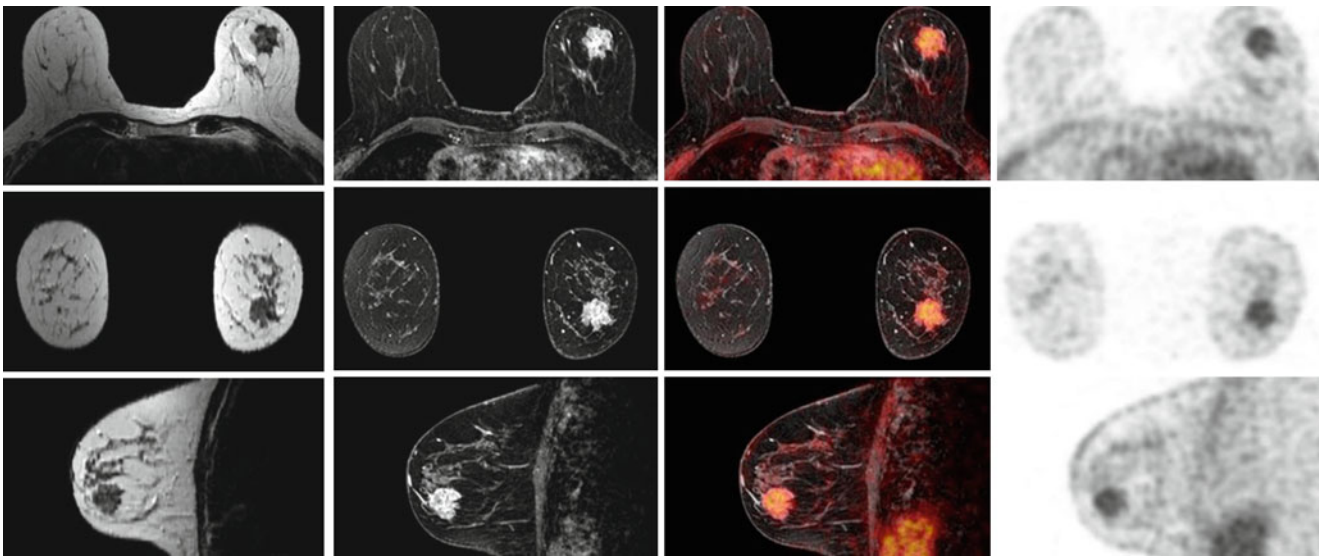

Fig. 6.31 Three orthogonal planes T2 TSE MRI (*far left*) and of venous phase of e-thrive MRI sequence after gadolinium injection (*left*), fused with PET (*middle*), and PET alone (*right*) showing gadolinium enhanced lesion with focal uptake of 18F-DOPA

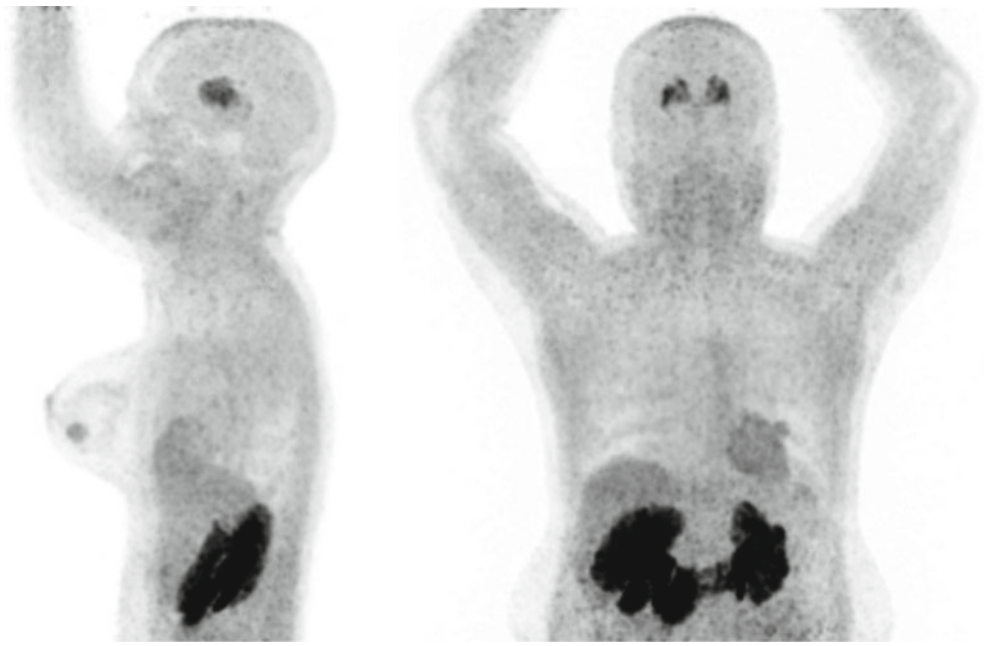

Fig. 6.32 Sagittal and coronal whole-body images of F18-DOPA study showing focal uptake of the left breast

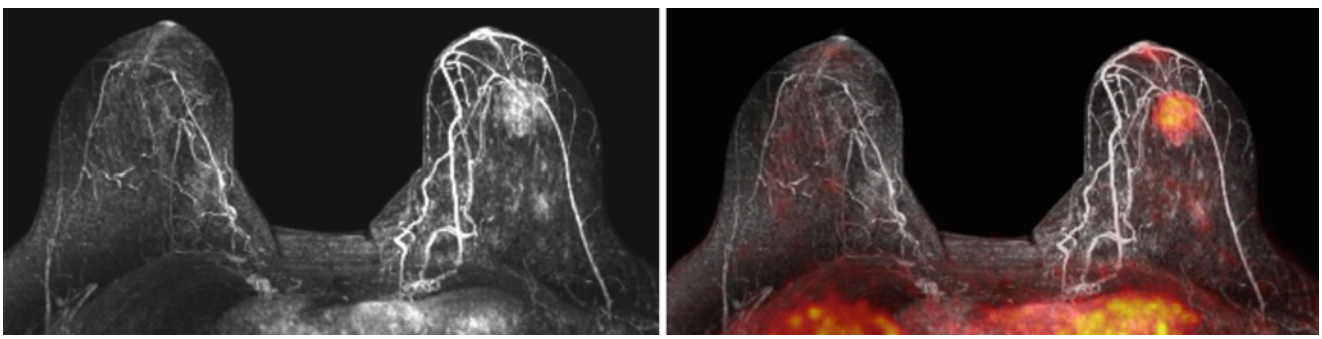

Fig. 6.33 Axial volume rendering of venous phase of e-thrive MRI sequence after gadolinium injection (*left*), and fused with 18F-DOPA PET (*right*) showing the location of left breast lesion

Multifocal IDC with Lymph Node Invasion

Clinical History

Forty-three-year-old patient with high grade (G3) cT2 N2 invasive ductal carcinoma (IDC) of the left breast. PET/MRI for staging disease was performed before neoadjuvant chemotherapy.

Imaging Technique

Whole-body PET acquired 60 min after injection of 375 MBq of 18F-FDG, 58 kg/157 cm patient, with 6.5 mmol/L of fasting glycemia. Whole body atMR (T1 weighted), supine position.

T2 TSE axial, 3D e-thrive native, arterial and venous post-gadolinium, and breast PET in a SENSE breast-coil, prone position.

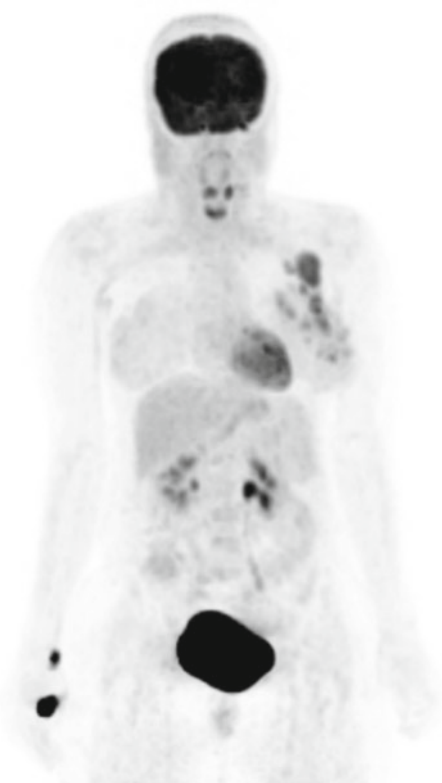

Fig. 6.34 MIP of the whole body PET, showing the left breast lesions with ipsilateral lymph node hypermetabolism

Findings

Whole body and breast PET/MR showed multifocal/multicentric hypermetabolic and enhanced tumoral extent of the left breast with massive ipsilateral axillar lymph node involvement, without controlateral breast lesion or distant metastasis.

Teaching Points

There is only very mild diffuse enhancement of the glandular tissue of the right breast. In the context of extensive tumor of the left breast, the absence of focal metabolic activity in the right breast PET makes the diagnosis of bilateral breast cancer very unlikely.

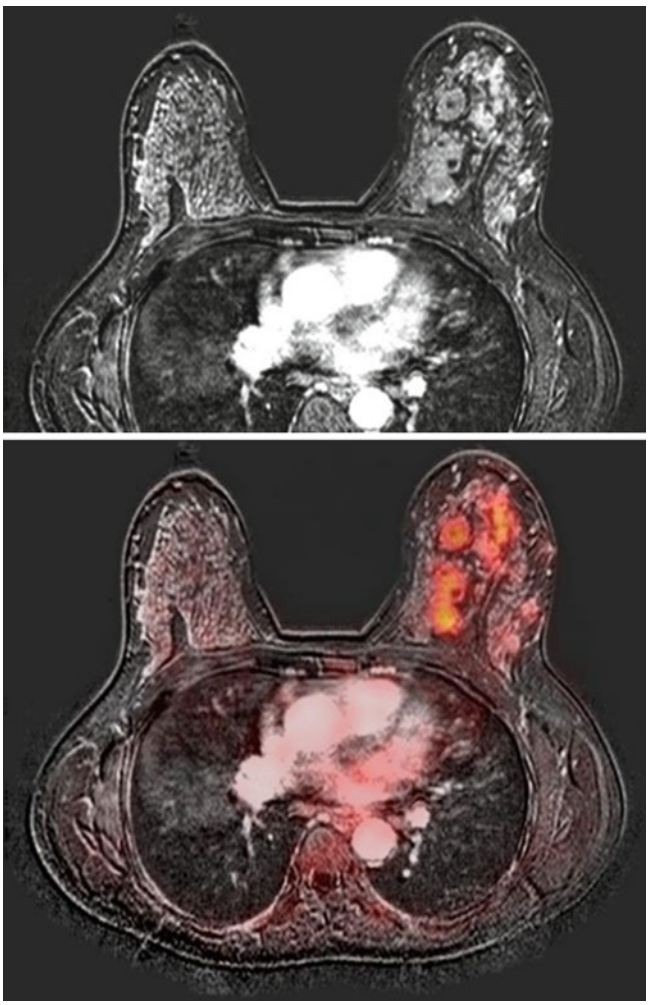

Fig. 6.35 E-thrive subtraction MRI sequence (*top*), fused with PET (*bottom*), both acquired in dedicated breast coil, showing the multifocal and multicentric left breast lesion, with important enhancement and hypermetabolism

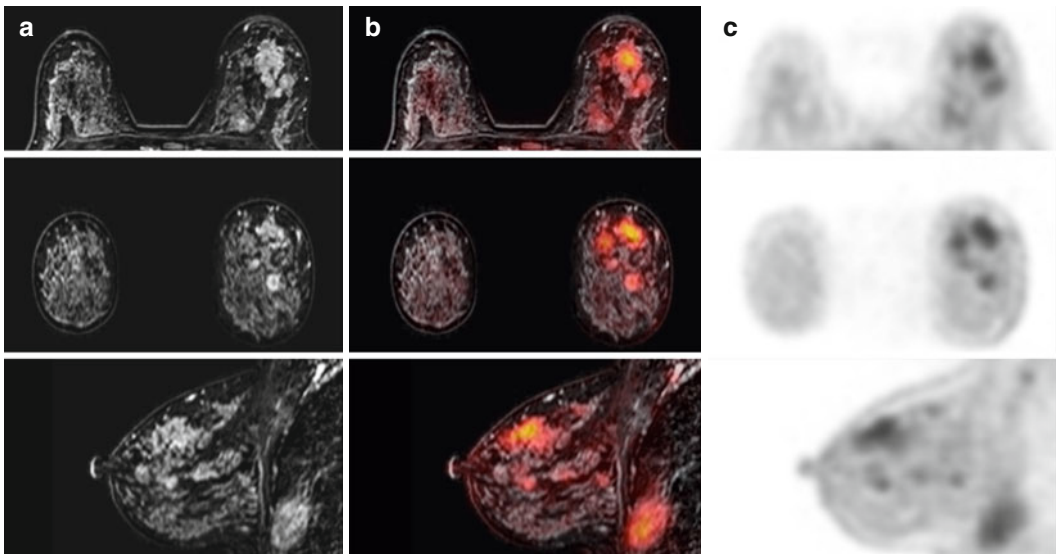

Fig. 6.36 *From left to right*, three orthogonal planes: (**a**) E-thrive subtraction MRI sequences, (**b**) fused PET/MRI, and (**c**) PET alone, acquired in the dedicated breast coil, showing the multifocal and multicentric left breast lesion, and axillary lymph node involvement

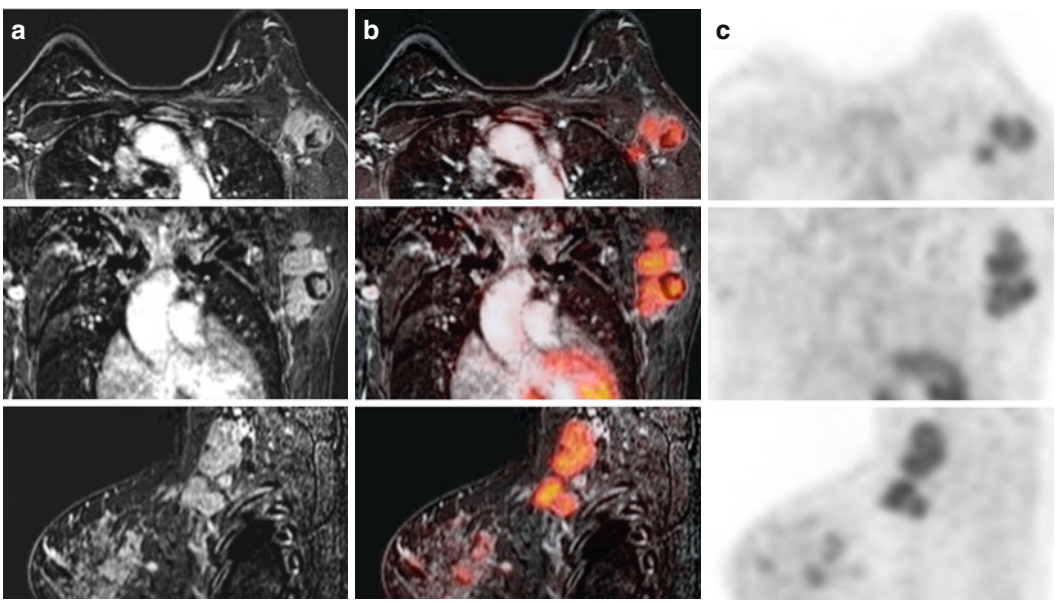

Fig. 6.37 E-thrive subtraction MRI sequence (**a**), fused PET/MRI (**b**), and PET alone (**c**), centered over the left axillar region showing the suspicious left axillar lymph nodes

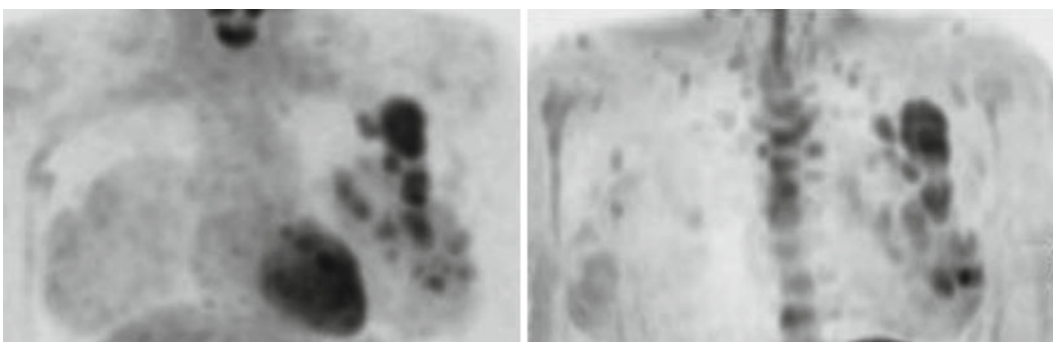

Fig. 6.38 Coronal views of the MIPS for PET on the *left*, vs Diffusion weighted (DWIBS) MRI sequence on the *right*, showing the multifocal tumor and suspicious axillary lymph nodes

Angiosarcoma of the Breast

Clinical History

Sixty-one-year-old patient with left breast carcinoma treated by lumpectomy and radiotherapy 10 years ago. Angiomatous lesions are noted on the skin at the junction of the inner quadrants of the left breast. Grade 2 angiosarcoma on CNB (core needle biopsy).

Imaging Technique

Whole-body PET acquired 60 min after injection of 375 MBq of 18F-FDG. Whole body atMR (T1 weighted), supine position.

3D e-thrive native, arterial and venous post-gadolinium, and breast PET in a SENSE breast-coil, prone position.

Findings

Breast MR showed suspected enhancement of the skin of the left inner inferior quadrant with 42-mm maximal diameter enhancement. PET images showed multifocal hypermetabolic lesions with the largest suspected lesion having a maximal diameter of 24 mm. Subsequent pathological examination of left mastectomy showed grade 2 angiosarcoma with 25 mm maximal size, dermal and hypodermal invasion.

Teaching Points

The area of contrast-enhancement on MRI is more extensive compared to the suspected lesion size. PET demonstrated more accurately the multifocal distribution and true tumor size. MRI could not separate the post radiation inflammatory component from undifferentiated tumor.

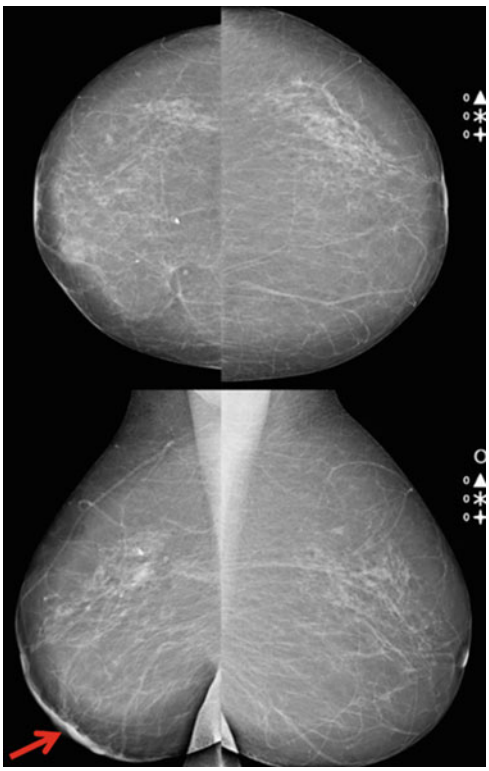

Fig. 6.39 Mammography of the right (*top*) and left (*bottom*) breast showing subcutaneous thickening at the location of the suspected lesion (*arrow*)

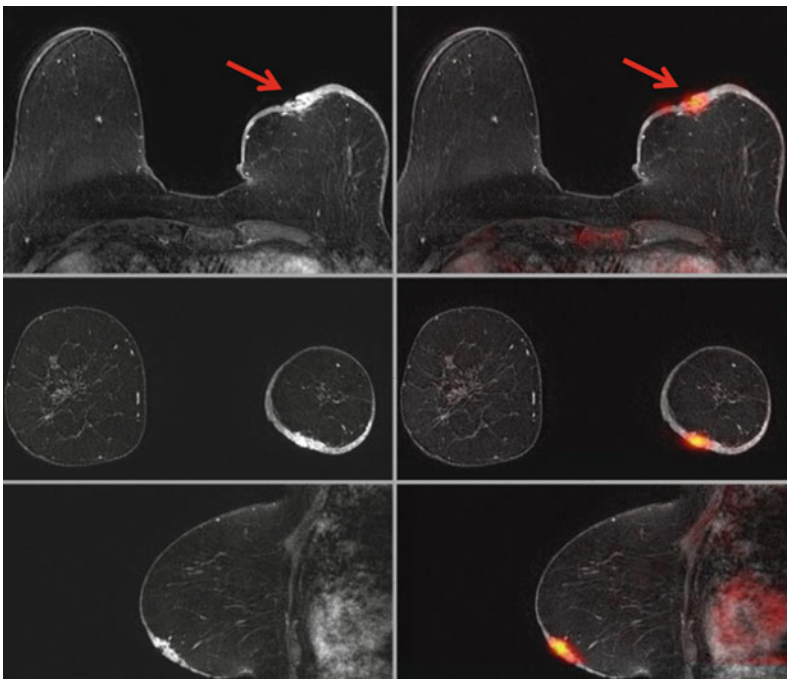

Fig. 6.40 Axial (*top*), coronal (*middle*) and sagittal (*bottom*) eThrive MRI images (*left*) fused with PET images (*right*) showing the multifocal distribution of the subcutaneous lesions (*arrows*)

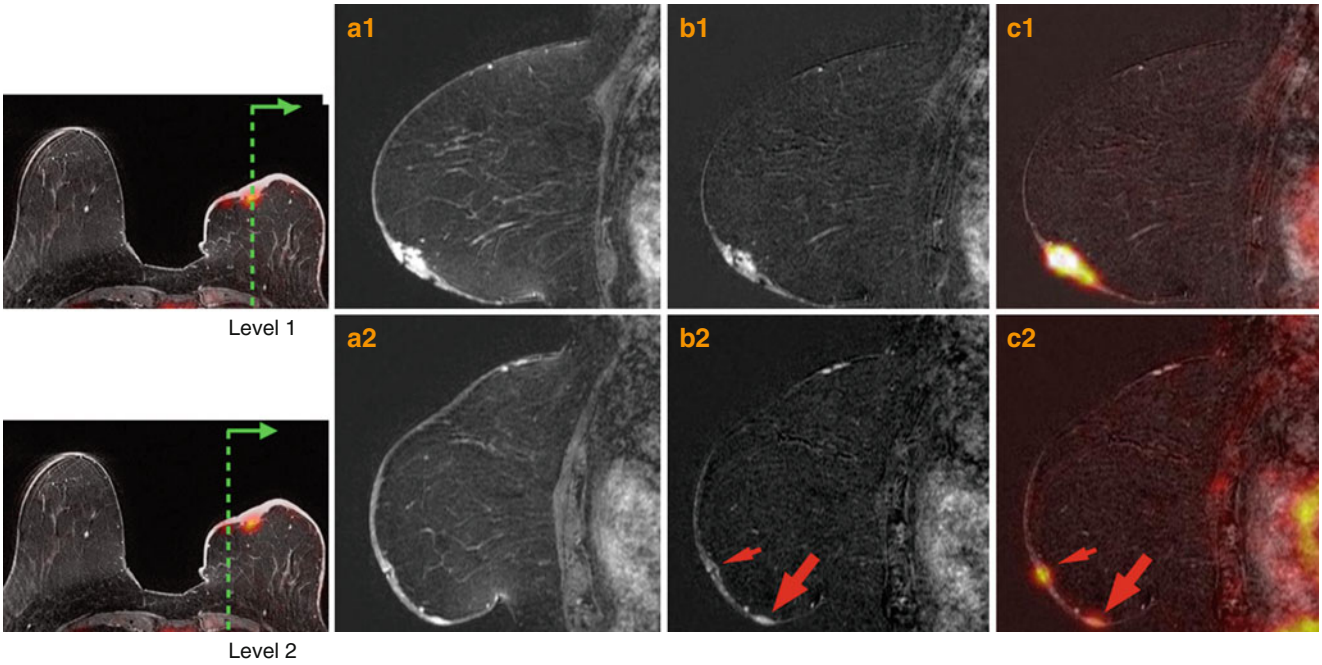

Fig. 6.41 Two levels of sagittal planes showing arterial (**a1**, **a2**), subtracted (**b1**, **b2**) and fused (**c1**, **c2**) images of the left breast showing the multifocal distribution of the lesions

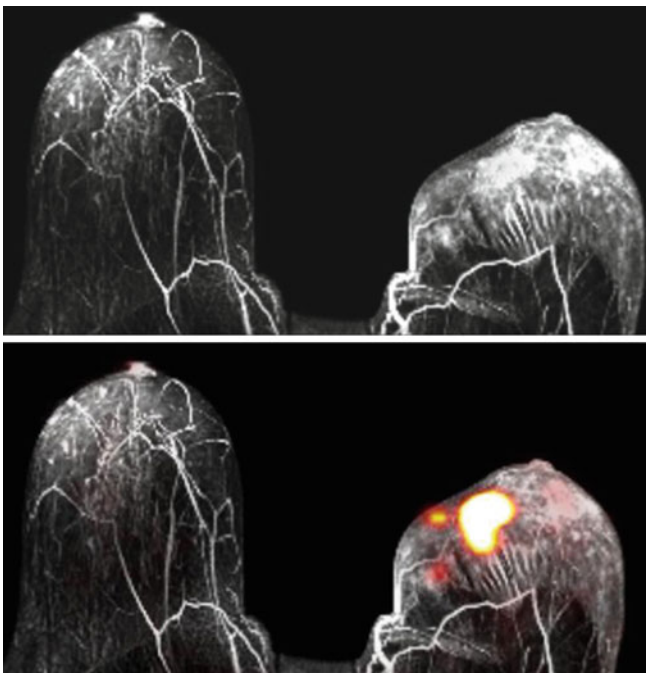

Fig. 6.42 Volume rendered images of contrast-enhanced MRI images (*top*) fused with PET images (*bottom*) of the left breast showing the multifocal distribution of the lesions

Fig. 6.43 Whole body MIP image of PET showing the left breast lesion but no other suspicious focal uptake of the tracer

Retroareolar ILC

Clinical History

Forty-five-year-old patient with retroareolar cT3 N1a invasive lobular carcinoma (ILC) grade 2 of the right breast. PET/MR was performed for staging.

Imaging Technique

Whole-body PET acquired 60 min after injection of 371 MBq of ^{18}F-FDG, 57 kg/157 cm patient, with 5 mmol/L of fasting glycemia. Whole body atMR (T1 weighted), supine position.

T2 TSE axial, 3D e-Thrive native, arterial and venous phase post-gadolinium, and breast PET in a SENSE breast-coil, prone position.

Findings

Breast PET/MR showed retroareolar, multicentric, 50 mm diameter tumor, with nipple invasion. Ipsilateral axillary lymphnode involvement was highly suspected on imaging. No contralateral breast lesion or distant metastatic extent was noted. Patient was treated by right mastectomy and axillary node dissection. On pathological examination, a 50-mm diameter invasive lobular carcinoma with dermal nipple showing the right breast retroareolar lesion with metastatic right axillary lymph nodes

Teaching Points

The glandular tissue of the right breast shows multinodular enhancement. In the context of contralateral tumor, the absence of high focal metabolic activity in PET in the left breast is an argument against the bilaterality of cancer. The hypermetabolism of right axillary lymph node was very suspicious, even though its diameter is <10 mm on MRI, which was found metastatic in pathological examination.

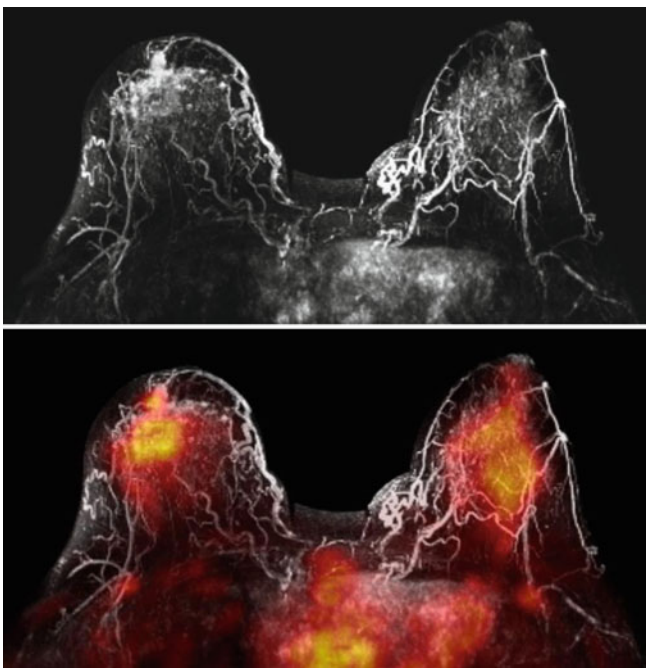

Fig. 6.44 3D reconstruction of arterial MRI e-Thrive sequence on the *top*, fused with FDG-PET at the *bottom*, showing the right breast retroareolar hypermetabolic lesion, with gadolinium uptake. This patient's breast tissues are dense, and therefore, there is a mild diffuse physiological FDG uptake in the opposite breast

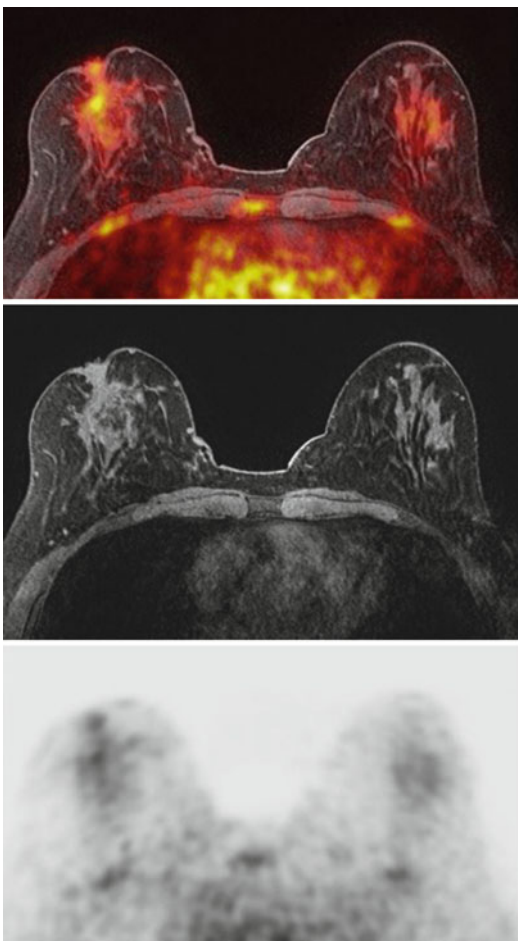

Fig. 6.45 *From the bottom to the top*, PET acquisition, native MRI e-Thrive sequence on the same level, and fusion of both modalities, showing the right breast lesion with nipple retraction

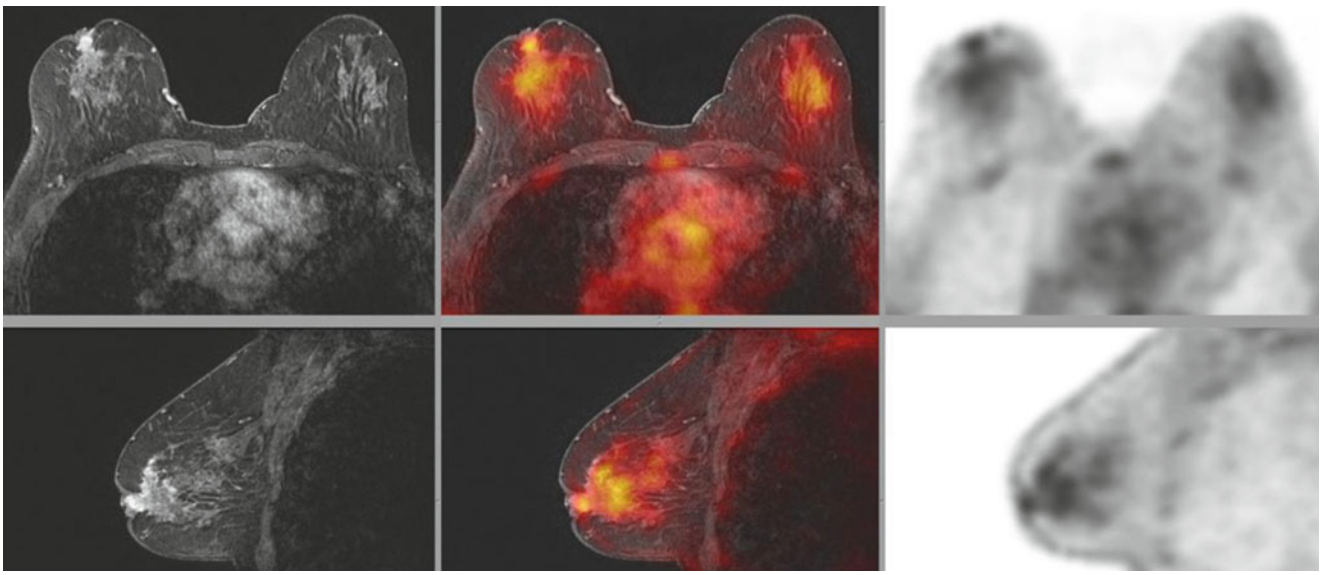

Fig. 6.46 Arterial MRI e-thrive sequence on the left, fused with the FDG-PET in axial (*top*) and sagittal (*bottom*) planes, showing the right breast retroareolar lesion

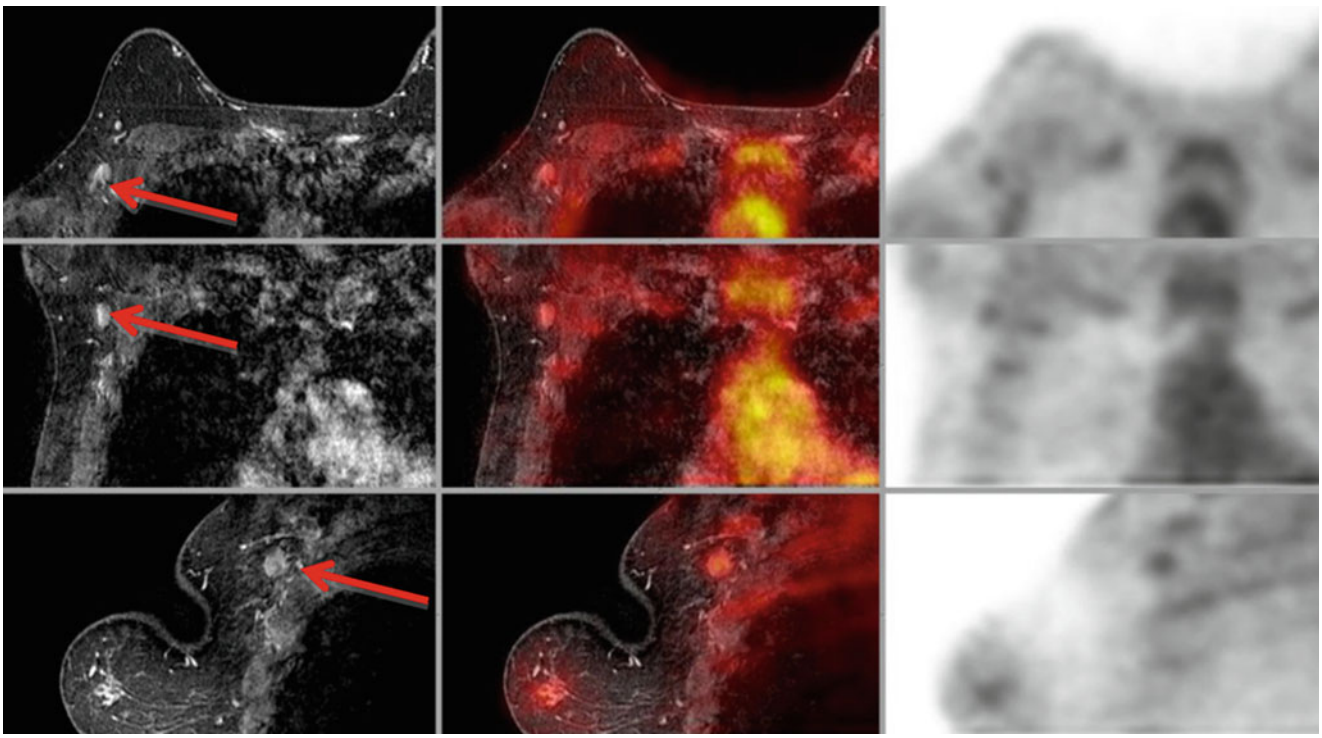

Fig. 6.47 Arterial phase e-thrive MRI sequence, fused with FDG-PET images in axial (*top*) coronal (*middle*) and sagittal (*bottom*) planes, showing one of the suspicious right axillary lymph nodes with mild to moderate PET uptake

Breast Cancer in Patient with Tuberculosis

Clinical History

Sixty-six-year-old patient presenting with breast cancer. A conventional mammography performed at an outside institution showed the primary lesion in the left breast.

Imaging Technique

PET/MR images acquired 76 min after iv injection of 294 MBq F-18 FLT (fluorothymidine), 65 kg. 1 bed × 10 min together with axial T1 TSE, axial DWI, axial DCE (KWIC), ax T1 TSE + Gd, axial T1 VIBE + Gs

PET/CT images acquired 101 min after iv injection of 371 MBq F-18 FDG (fluoroglucose), 65 kg. 8 beds × 3 min with intravenous contrast

Findings

FLT-PET/MR and FDG-PET/CT for primary staging show a lesion in the left breast with high tracer uptake. In addition especially CT demonstrates multiple intrapulmonary lesions with positive uptake in the FLT and FDG-dataset. Due to previously known tuberculosis, the morphological appearance and the increased metabolism in PET the clinical suspicion was reactivated tubercular infiltration. The following biopsy confirmed reactivated tuberculosis.

Teaching Points

PET/MR imaging is suitable for whole body staging investigations. In this case both examinations (FDG-PET/CT and FLT-PET/MR) showed a good correlation between morphology and tracer uptake in the breast. However the FDG-PET/CT leads to a better morphological discrimination of the pulmonary lesions demonstrating the superiority of CT over MR for pulmonary pathologies.

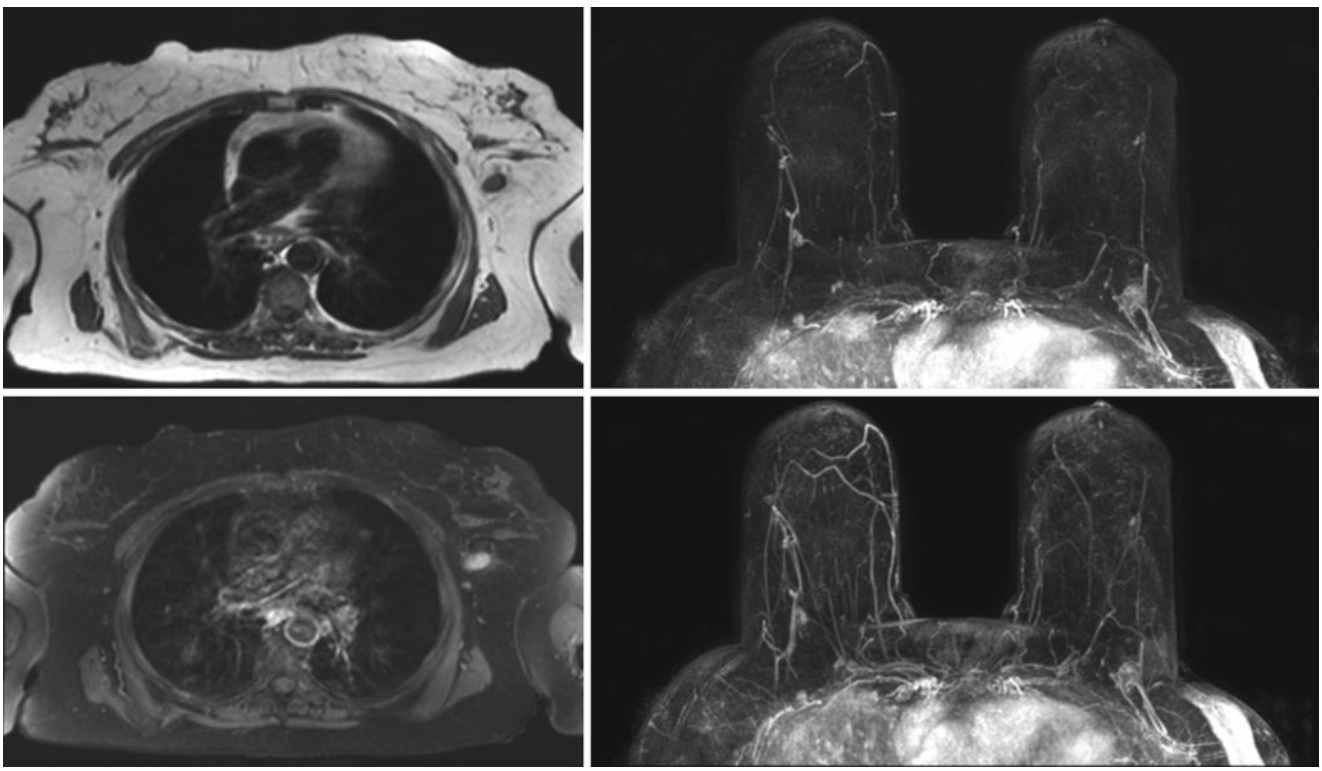

Fig. 6.48 *Left side*: Native T1w TSE demonstrates a nodular lesion in the left outer quadrant with intense enhancement in the T1w fs images. In addition several faint enhancing pulmonary lesions were found but difficult to discriminate on MR. *Right side*: Axial MIP projections nicely outline the whole breasts and demonstrate early as well as late contrast enhancement of the lesion

Fig. 6.49 *Left*: Contrast enhanced GRE fs-sequence in the arterial phase shows a hypervascularized lesion in the left outer quadrant; *middle*: moderate focal FLT-uptake is found in the corresponding area; *right*: fused PET/MR-image demonstrates a good co-registration between both datasets

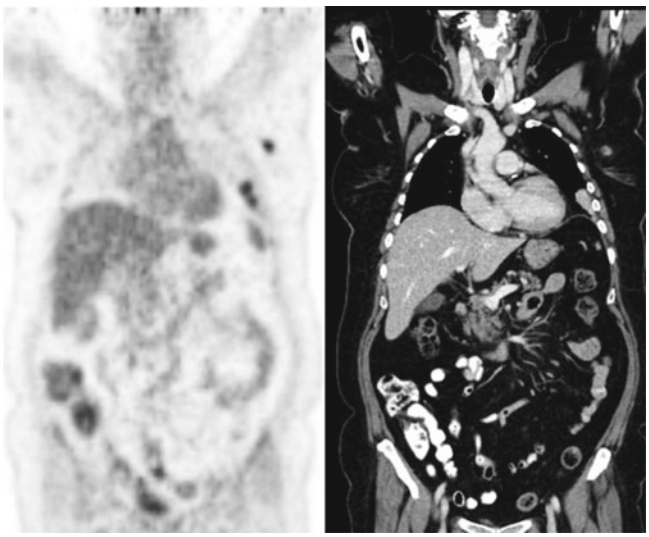

Fig. 6.50 FDG-PET and morphological contrast enhanced CT correlation shows the primary tumor of the left breast and in addition multiple pulmonary lesions, the biggest in the area of the basal left lung

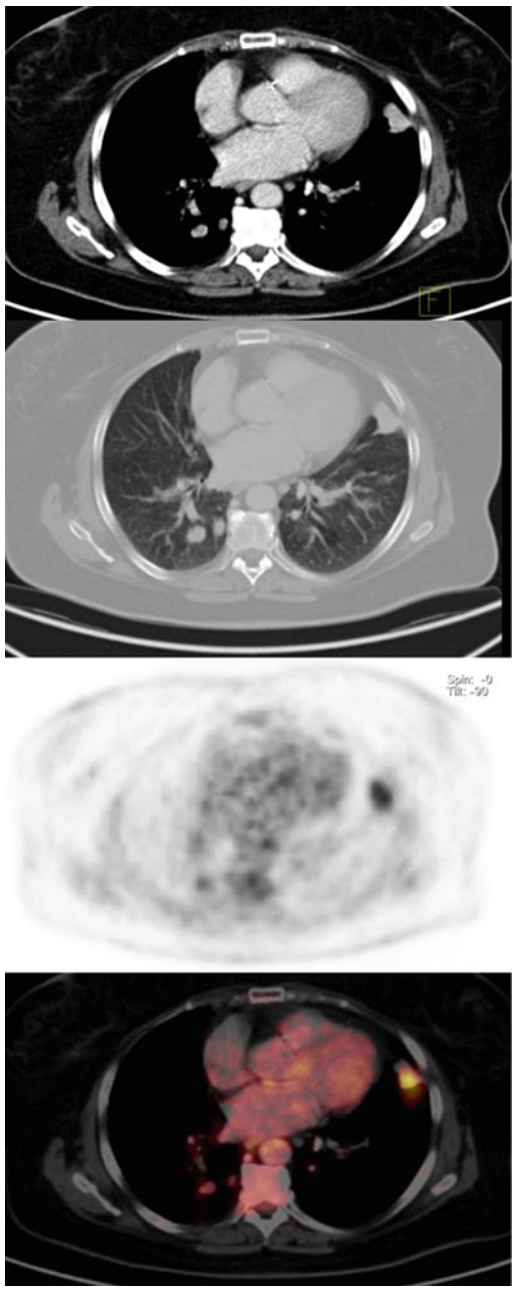

Fig. 6.51 *From top to bottom*: CT soft-tissue windows, CT lung window, axial PET, axial fused image: Clear anatomical outline of the pulmonary lesion is given by the CT dataset. The lesions show moderate focal uptake in FDG-PET indicating an active inflammatory process in known tuberculosis. However lung metastases could not be excluded in a patient with breast cancer

Triple-Negative Breast Cancer

Clinical History

Sixty-nine-year-old patient presenting with triple negative Breast Cancer on the right side. PET/MR indication: staging before neoadjuvant chemotherapy and early response imaging after first chemotherapy cycle.

Imaging Technique

First examination: Whole body PET/MR images acquired 79 min after iv injection of 316 MBq F-18 FLT (fluorothymidine), 72 kg.

Early response 2 weeks after the first cycle of chemotherapy: Whole body PET/MR images acquired 67 min after iv injection of 271 MBq F-18 FLT (fluorothymidine), 70 kg.

In both examinations 1 bed × 10 min together with axial T2 Haste fs, axial Vibe fs + Gd dynamic.

Findings

The staging examination shows high uptake of FLT in PET in the lower inner quadrant of the right breast. The MR images shows a pathological contrast enhancement of this lesion with a central radiopaque marker. Furthermore, a very low tracer uptake showed in projection on an enlarged lymph node in the area of the right internal mammary artery.

Early response imaging 2 weeks after first cycle of chemotherapy demonstrates a reduction of size in MRI and a significant decrease of tracer uptake of the primary lesion.

Teaching Points

The combination of PET and MR imaging can lead to a more accurate discrimination of malignant lesions and their proliferation or metabolic activity. In this case, additional FLT-PET information shows a significant reduce of proliferation after one cycle of chemotherapy in correlation to the decrease in size in MRI in the sense of a good response to chemotherapy.

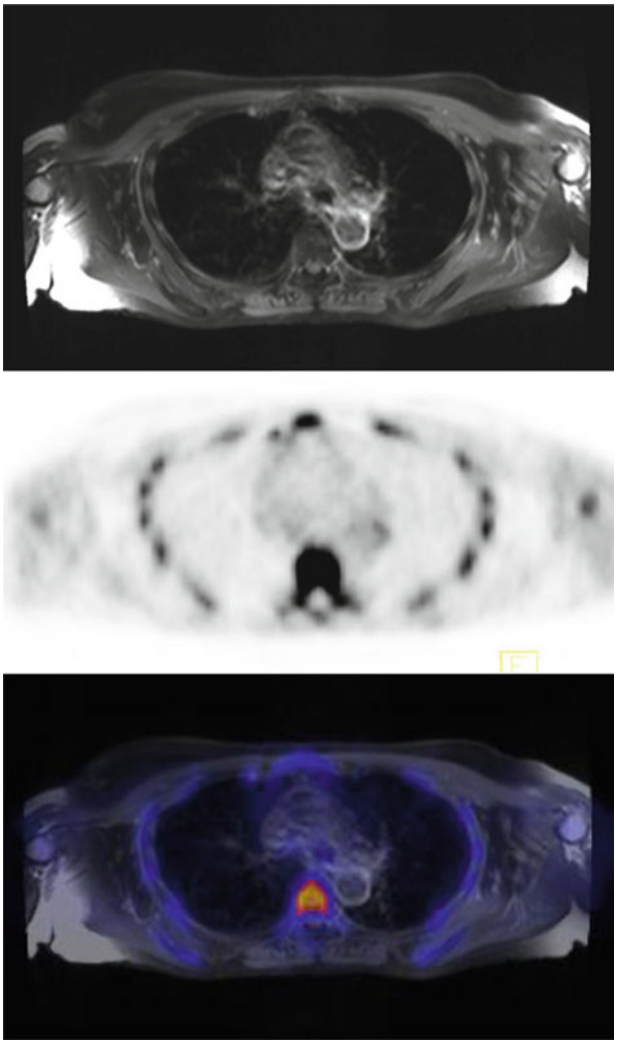

Fig. 6.52 Low FLT uptake of a lymph node in the area of the internal mammary artery to the right. The MR imaging (T1w fs + Gd) shows an enlarged lymph node with pathological contrast enhancement

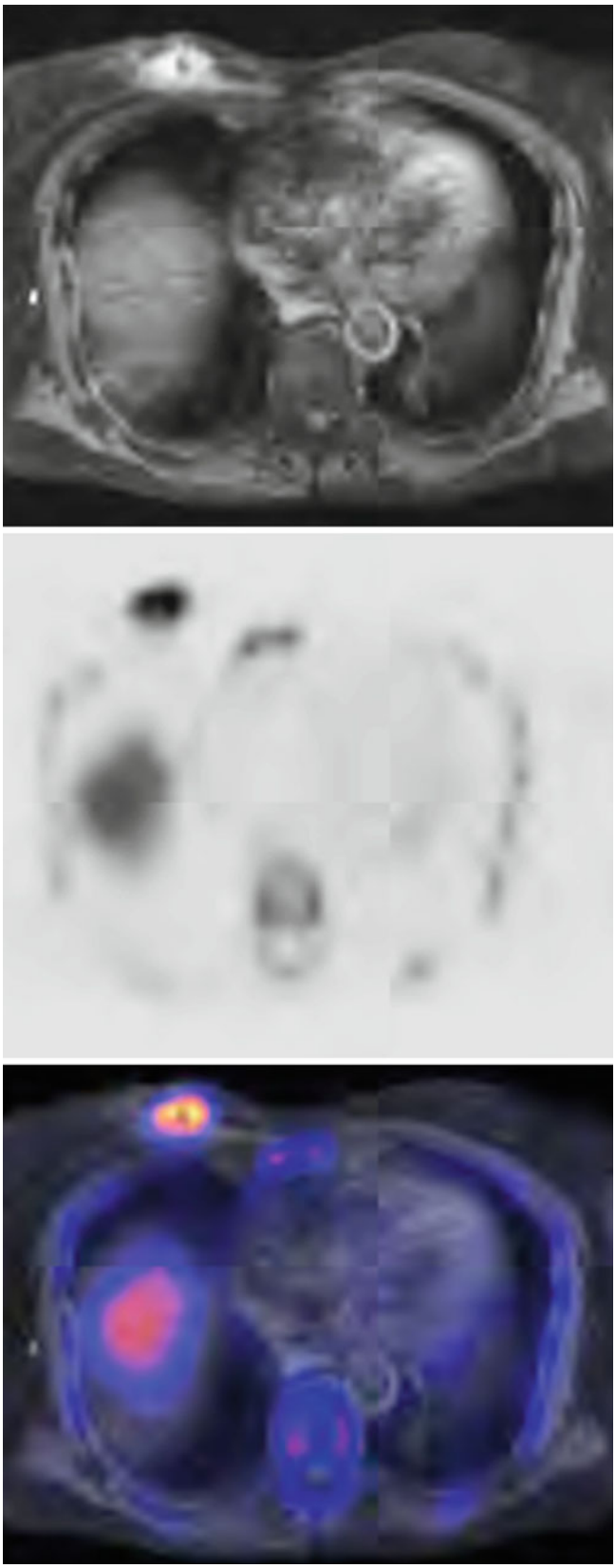

Fig. 6.53 Axial views. *From top to bottom*: MRI (ax T1w fs+Gd); FLT-PET Scan; PET/MR Fusion showing the staging images with a perfect co-registration of the lesion in the right breast before chemotherapy

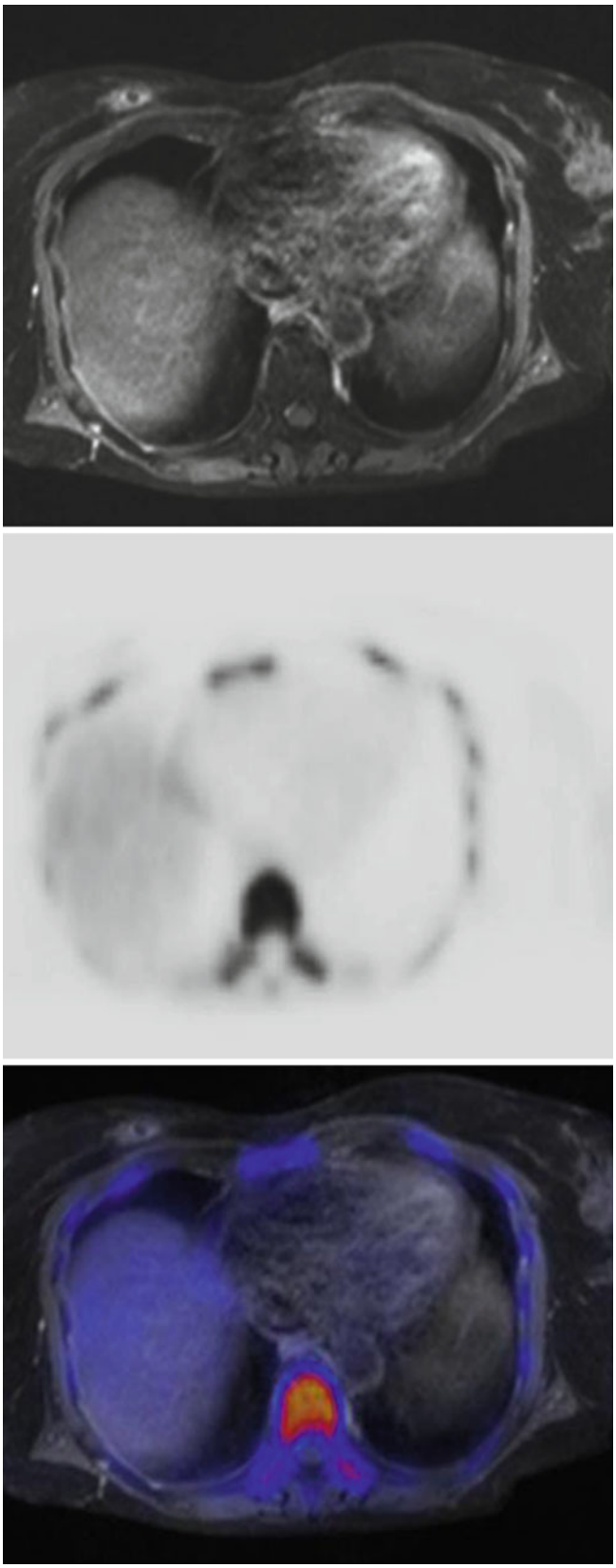

Fig. 6.54 Same sets of axial views acquired after chemotherapy shows no more or even a very low FLT uptake and a decrease of size 2 weeks after first cycle of chemotherapy

References

1. Kuhl C (2007) The current status of breast MR imaging. Part I. Choice of technique, image interpretation, diagnostic accuracy, and transfer to clinical practice. Radiology 244(2):356–378
2. Kuhl CK (2007) Current status of breast MR imaging. Part 2. Clinical applications. Radiology 244(3):672–91
3. Biglia N et al (2011) Role of MRI (magnetic resonance imaging) versus conventional imaging for breast cancer presurgical staging in young women or with dense breast. Eur J Surg Oncol 37(3): 199–204
4. Moy L et al (2010) Role of fusion of prone FDG-PET and magnetic resonance imaging of the breasts in the evaluation of breast cancer. Breast J 16(4):369–376
5. Koolen BB et al (2012) 18F-FDG PET/CT as a staging procedure in primary stage II and III breast cancer: comparison with conventional imaging techniques. Breast Cancer Res Treat 131(1):117–126
6. Alberini JL et al (2009) 18F-fluorodeoxyglucose positron emission tomography/computed tomography (FDG-PET/CT) imaging in the staging and prognosis of inflammatory breast cancer. Cancer 115(21):5038–5047
7. Carkaci S et al (2009) Retrospective study of 18F-FDG PET/CT in the diagnosis of inflammatory breast cancer: preliminary data. J Nucl Med 50(2):231–238
8. Pennant M et al (2010) A systematic review of positron emission tomography (PET) and positron emission tomography/computed tomography (PET/CT) for the diagnosis of breast cancer recurrence. Health Technol Assess 14(50):1–103
9. Ueda S et al (2011) Early metabolic response to neoadjuvant letrozole, measured by FDG PET/CT, is correlated with a decrease in the Ki67 labeling index in patients with hormone receptor-positive primary breast cancer: a pilot study. Breast Cancer 18(4): 299–308
10. Duch J et al (2012) PET/CT with [18F] fluorodeoxyglucose in the assessment of metabolic response to neoadjuvant chemotherapy in locally advanced breast cancer. Q J Nucl Med Mol Imaging 56(3):291–298
11. Duch J et al (2009) 18F-FDG PET/CT for early prediction of response to neoadjuvant chemotherapy in breast cancer. Eur J Nucl Med Mol Imaging 36(10):1551–1557
12. Vargas MI et al (2013) Approaches for the optimization of MR protocols in clinical hybrid PET/MRI studies. MAGMA 26(1):57–69